Vehicle Dynamics 4L150

Eindhoven University of Technology
Mechanical Engineering - Dynamics & Control

I.J.M. Besselink, A.J.C. Schmeitz
hand-out: Vertical Dynamics 2008

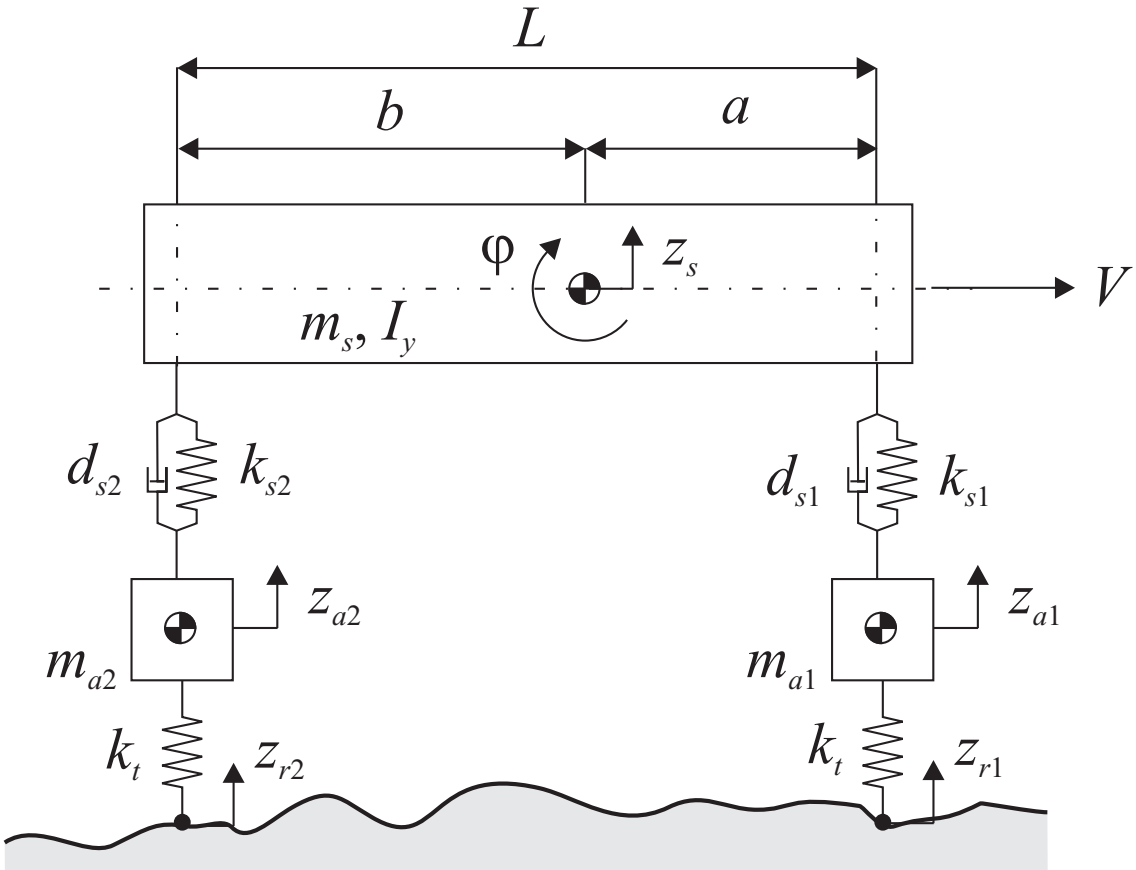

Contents

Chapter 1

Introduction to vehicle dynamics

The research field known as vehicle dynamics studies the vehicle behavior for various driving conditions. It is concerned with the movements and vibrations of cars, trucks, busses and special purpose vehicles while driving over road surfaces. Two main research areas can be distinguished:

- ride (comfort)
- handling

Ride is about isolating the driver from vibrations occurring as a result of operating the vehicle (sources: engine, road, tyre, driveline). When driving, the vehicle experiences a broad spectrum of vibrations. These vibrations are transmitted to the passengers either by tactile, visual or aural paths. In general the term 'ride' is used in reference to tactile and visible vibrations, while the aural vibrations are characterized as 'noise'. In the frequency domain, we may classify the spectrum of vibrations below 80 Hz important for ride and that from 25 Hz to 20 kHz as noise. The 80 Hz boundary is the upper limit of the frequency range according to which the vibration comfort of the human body is usually assessed [2]. The 25 Hz and 20 kHz boundaries are approximately the lower and upper frequency thresholds of human hearing. Although reduction of noise is also about isolating the driver from disturbances, it is generally not studied in classical vehicle dynamics.

Handling is concerned largely with the behavior of the vehicle in response to driver demands (steering, braking, accelerating). To follow an arbitrary course, the driver continuously varies both path curvature and velocity. Handling not only encompasses the objective properties of the vehicle like e.g. cornering performance, accelerating/braking performance and (dynamic) stability, but it also considers the system performance of the driver-vehicle combination. This means that the vehicle qualities that feed back to the driver affecting the ease of the driving task or affecting the driver's ability to maintain control are studied as well (e.g.: straight line stability, on-center feel).

Although above a split is made between ride and handling, in reality many interactions exist. For example, when driving over uneven road surfaces, not only the vehicle body and the passengers are excited (ride), but also the vertical force acting on the tyres varies, which has an influence on the handling performance of the vehicle. One can imagine that one of the difficulties in vehicle dynamics is the complexity of the various interactions. Although, the most relevant components of the vehicle that are studied are the tyres, suspension, steering system and brake system, it should be clear that these components cannot be designed without taking the full vehicle behavior and its surrounding into consideration. In vehicle design, a compromise has to be made between handling and ride performance.

Nowadays, the following two trends can be observed in the field of vehicle dynamics:

- Shift towards 'virtual prototyping'
- Introduction of sophisticated control systems to improve the vehicle behavior

As a result of the increase in computing power, virtual prototyping is becoming an integral part of the vehicle design process. Today, it is possible to build detailed full vehicle models (see figure 1.1) from individually built accurately modeled components. These

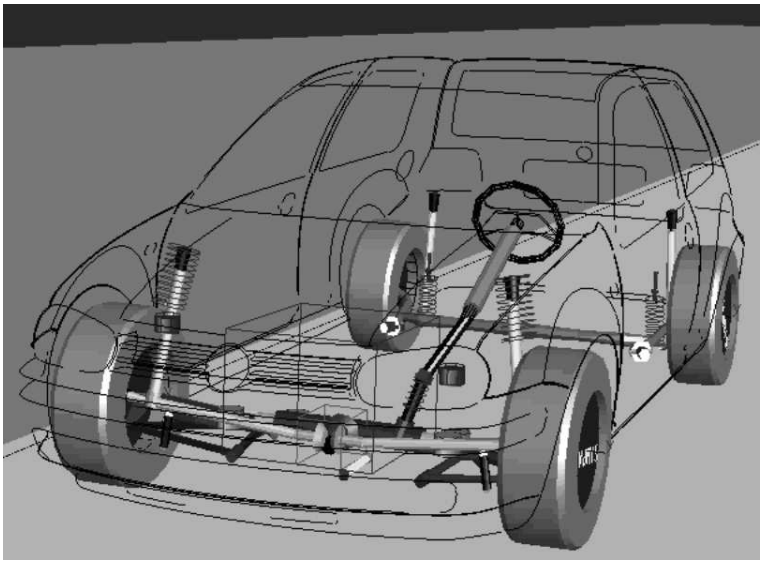

Figure 1.1: Detailed full vehicle multibody model (courtesy of SIMPACK)

models allow the engineer to simulate and evaluate vehicle behavior before a real prototype is built. In the field of vehicle dynamics multi-body simulation packages like Adams, SIMPACK and DADS are widely used. Although, virtual prototyping has significantly reduced the development times of vehicles, we are still far from the ideal situation that only a few prototypes have to be built for validating the virtual prototype car. Consequently, there is still an ever-increasing demand in more detailed/accurate simulation models. A herewith-related trend is a shift from subjective to objective hardware testing. Objective testing may however require a detailed knowledge of driver perception and behavior. For example: what engineering parameters are related to comfort or steering feel?

As a result of the advances in control engineering, many systems to improve the vehicle dynamic behavior have been introduced. Also here, the rapid development of computers/electronics in the past years plays an important roll. For example, the concept of ABS (anti-lock braking system) dates back to the 1930s, but only recently almost every car on the market is equipped with ABS. Below, a list of systems to improve the vehicle dynamic behavior is given:

- anti-lock braking system (ABS)
- traction control (ASR, TCS)
- handling stability improvement systems (ESP, VDC)
- adjustable shock absorbers (EDC)
- active front steering (AFS)
- adaptive cruise control (ACC)

It is not difficult to understand that the more systems are installed in the vehicle, the number of actuators, sensors and controllers increases with as result that the complexity of controlling the vehicle's motions increases. Further, the role of a number of components is becoming operationally critical so that a fault might result in a failure. To increase the degree of fault tolerance in vehicle control, a supervisory controller is necessary that 'conducts' the full orchestra of individual active controllers. In such supervisory controller, the reconfiguration of the control activities is determined in case of component degradation or malfunctioning. The development of such a supervisory controller is one of the main challenges that we are facing today. Besides, new control systems like steer-by-wire will be introduced in the near future.

Chapter 2

Vertical Dynamics

2.1 Introduction

In this series of lectures, the vertical dynamics of the vehicle is studied. Simple mathematical models are derived and applied to obtain the vehicle dynamic response to uneven road surfaces. Simulation results are analyzed both in the time domain and in the frequency domain. In addition, an engineering parameter to judge ride comfort is defined: the ride comfort index. The design requirements for a suspension are discussed and it is shown that a compromise has to be made between the various requirements. Also a control strategy for a semi-active suspension where the damping coefficient is adjusted is presented. Further, nonlinear behavior that exists in real suspension systems is briefly discussed.

2.2 The quarter car vehicle model

At the most basic level, the essential vertical dynamics of every road vehicle can be represented by a quarter car vehicle model (figure 2.1) that moves with forward velocity V over a road surface. The model consists of a sprung mass m_s supported on a suspension, which in turn is connected to the unsprung mass m_a of the vehicle. The suspension has stiffness k_s and damping d_s properties. The tyre is represented as a spring with stiffness k_t. Input to the model is the road profile height z_r.
In deriving the equations of motion of the model, we only consider small variations about the equilibrium position. This means that the gravity forces can be disregarded (a formal proof will be given further on in this section). First, a free body diagram is created in figure 2.1. From this, expressions for the forces in the suspension and the tyre can be derived:

$$\Delta F_s = k_s(z_s - z_a) + d_s(\dot{z}_s - \dot{z}_a) \tag{2.1}$$

$$\Delta F_z = k_t(z_a - z_r) \tag{2.2}$$

In these equations z_s and z_a are small displacements about the equilibrium position of the sprung and unsprung masses, respectively, and z_r the road height. The equation of motion of the sprung and unsprung masses equal, respectively:

$$m_s\ddot{z}_s = -\Delta F_s = -k_s(z_s - z_a) - d_s(\dot{z}_s - \dot{z}_a) \tag{2.3}$$

$$m_a\ddot{z}_a = \Delta F_s - \Delta F_z = k_s(z_s - z_a) + d_s(\dot{z}_s - \dot{z}_a) - k_t(z_a - z_r) \tag{2.4}$$

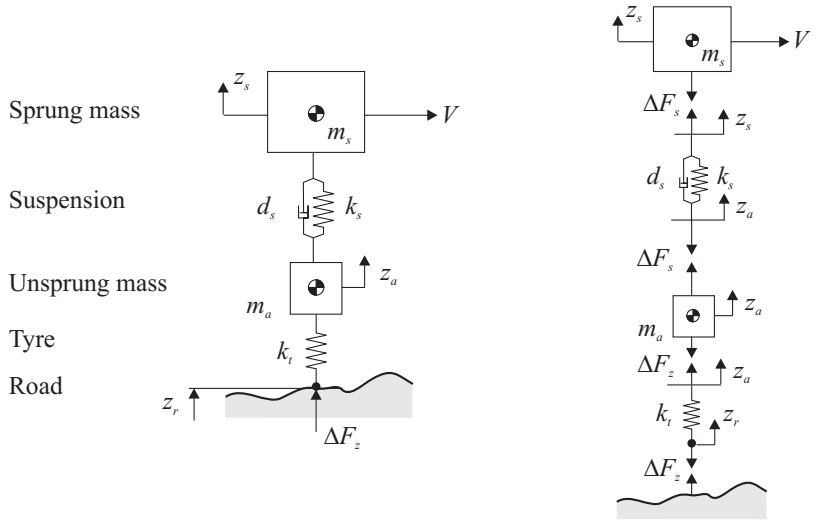

Figure 2.1: Quarter car vehicle model and free body diagram

If we also want to account for the large displacements as a result of the vertical load, we have to consider the gravitational forces. The total displacements of the sprung and unsprung masses can be written as the sum of a stationary component and a small deviation about the equilibrium position:

$$z_{st} = z_{s0} + z_s \tag{2.5}$$

$$z_{at} = z_{a0} + z_a \tag{2.6}$$

where the subscripts 't' and '0' are used to indicate the 'total' and 'stationary' displacements. Note that all displacements equal zero if the gravity forces equal zero. The free body diagram of the system for large displacements is shown in figure 2.2.

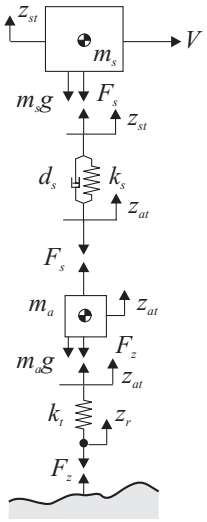

Figure 2.2: Free body diagram of quarter car vehicle model with gravity added

Again, we obtain the expressions for the forces in the suspension and the tyre from the free body diagram:

$$F_s = k_s(z_{st} - z_{at}) + d_s(\dot{z}_{st} - \dot{z}_{at}) \tag{2.7}$$

$$F_z = k_t(z_{at} - z_r) \tag{2.8}$$

Or, by substitution of equations (2.5) and (2.6):

$$F_s = k_s(z_{s0} + z_s - z_{a0} - z_a) + d_s(\dot{z}_s - \dot{z}_a) \tag{2.9}$$

$$F_z = k_t(z_{a0} + z_a - z_r) \tag{2.10}$$

Note that the time derivatives of stationary values are zero! The equations of motion of the sprung and unsprung masses now become:

$$m_s\ddot{z}_s = -F_s - m_s g \tag{2.11}$$

$$m_a\ddot{z}_a = F_s - F_z - m_a g \tag{2.12}$$

Or by substitution of the forces:

$$m_s\ddot{z}_s = -k_s(z_{s0} + z_s - z_{a0} - z_a) - d_s(\dot{z}_s - \dot{z}_a) - m_s g \tag{2.13}$$

$$m_a\ddot{z}_a = k_s(z_{s0} + z_s - z_{a0} - z_a) + d_s(\dot{z}_s - \dot{z}_a) - k_t(z_{a0} + z_a - z_r) - m_a g \tag{2.14}$$

In the stationary situation, these equations reduce to:

$$m_s g = -k_s(z_{s0} - z_{a0}) \tag{2.15}$$

$$m_a g = k_s(z_{s0} - z_{a0}) - k_t z_{a0} \tag{2.16}$$

The stationary displacements can be found by combining these equations:

$$z_{a0} = -\frac{(m_a + m_s)g}{k_t} \tag{2.17}$$

$$z_{s0} = -\frac{m_s g}{k_s} + z_{a0} \tag{2.18}$$

If we now substitute equations (2.15) and (2.16) in the equations of motion (equations (2.13) and (2.14)), the equations of motion for small displacements about the equilibrium position are found again (equations (2.3) and (2.4)):

$$m_s\ddot{z}_s = -k_s(z_s - z_a) - d_s(\dot{z}_s - \dot{z}_a) \tag{2.19}$$

$$m_a\ddot{z}_a = k_s(z_s - z_a) + d_s(\dot{z}_s - \dot{z}_a) - k_t(z_a - z_r) \tag{2.20}$$

In order to analyse the model, the system is written in state-space form. The generic form for a state-space representation of a system is given by:

$$\dot{\mathbf{x}} = \mathbf{A}\mathbf{x}(t) + \mathbf{B}\mathbf{u}(t) \tag{2.21}$$

$$\mathbf{y} = \mathbf{C}\mathbf{x}(t) + \mathbf{D}\mathbf{u}(t) \tag{2.22}$$

where:

$\mathbf{x}(t)$	=	$(n \times 1)$ state vector where n is the number of states or system order
$\mathbf{u}(t)$	=	$(r \times 1)$ input vector, where r is the number of input functions
$\mathbf{y}(t)$	=	$(p \times 1)$ output vector, where p is the number of outputs
$\mathbf{A}$	=	$(n \times n)$ system matrix
$\mathbf{B}$	=	$(n \times r)$ input matrix
$\mathbf{C}$	=	$(p \times n)$ output matrix
$\mathbf{D}$	=	$(p \times r)$ matrix that represents any direct connection between the input and the output

To write the equations of motion of the quarter car vehicle model in state-space form, we first write down the state vector:

$$\mathbf{x} = \begin{bmatrix} \dot{z}_s & \dot{z}_a & z_s & z_a \end{bmatrix}^T \tag{2.23}$$

In our model, the input is the road surface height z_r. Consequently, the input vector $\mathbf{u}$ equals:

$$\mathbf{u} = z_r \tag{2.24}$$

By using equations (2.3) and (2.4), equation (2.21) can be written as:

$$\begin{bmatrix} \ddot{z}_s \\ \ddot{z}_a \\ \dot{z}_s \\ \dot{z}_a \end{bmatrix} = \begin{bmatrix} -\frac{d_s}{m_s} & \frac{d_s}{m_s} & -\frac{k_s}{m_s} & \frac{k_s}{m_s} \\ \frac{d_s}{m_a} & -\frac{d_s}{m_a} & \frac{k_s}{m_a} & -\frac{k_s+k_t}{m_a} \\ 1 & 0 & 0 & 0 \\ 0 & 1 & 0 & 0 \end{bmatrix} \begin{bmatrix} \dot{z}_s \\ \dot{z}_a \\ z_s \\ z_a \end{bmatrix} + \begin{bmatrix} 0 \\ \frac{k_t}{m_a} \\ 0 \\ 0 \end{bmatrix} z_r \tag{2.25}$$

As will be discussed later, interesting outputs for designing a vehicle suspension system are the vertical acceleration of the sprung mass $\ddot{z}_s$, the dynamic tyre load ΔF_z and the suspension travel Δz_s. The vertical acceleration is important for evaluating ride comfort, the dynamic tyre load for road holding and the suspension travel for space requirements. Furthermore, the displacements of the sprung and unsprung masses are added as outputs. Therefore, the output vector reads:

$$\mathbf{y} = \begin{bmatrix} \ddot{z}_s & \Delta F_z & \Delta z & z_s & z_a \end{bmatrix}^T \tag{2.26}$$

To find the state-space output equation, first the separate output equations have to be written down. The equation for the vertical acceleration of the sprung mass can be obtained from equation (2.3):

$$\ddot{z}_s = -\frac{k_s}{m_s}(z_s - z_a) - \frac{d_s}{m_s}(\dot{z}_s - \dot{z}_a) \tag{2.27}$$

The equation for the dynamic tyre load equals equation (2.2) and the equation for the suspension travel reads:

$$\Delta z = z_a - z_s \tag{2.28}$$

Notice that a compression of the suspension spring (jounce) has a positive sign and an extension of the suspension spring (rebound) has a negative sign. By using equations (2.27), (2.2) and (2.28), equation (2.22) equals:

$$\begin{bmatrix} \ddot{z}_s \\ \Delta F_z \\ \Delta z \\ z_s \\ z_a \end{bmatrix} = \begin{bmatrix} -\frac{d_s}{m_s} & \frac{d_s}{m_s} & -\frac{k_s}{m_s} & \frac{k_s}{m_s} \\ 0 & 0 & 0 & -k_t \\ 0 & 0 & -1 & 1 \\ 0 & 0 & 1 & 0 \\ 0 & 0 & 0 & 1 \end{bmatrix} \begin{bmatrix} \dot{z}_s \\ \dot{z}_a \\ z_s \\ z_a \end{bmatrix} + \begin{bmatrix} 0 \\ k_t \\ 0 \\ 0 \\ 0 \end{bmatrix} z_r \tag{2.29}$$

Next, the behavior of the quarter car vehicle model is investigated. The numerical values of the vehicle parameters that are used in the analyses are depicted in table 2.1.

To analyse the response properties of the vehicle, we consider the transfer functions of the vertical displacements of the sprung and unsprung masses on the road input z_r. In figure 2.3, these transfer functions are plotted. It is observed that for very low frequencies both the sprung and unsprung masses follow the road profile height, i.e. the magnitude of

Table 2.1: Quarter car vehicle model parameters

Category	Parameters
Masses	$m_s = 400$ kg; $m_a = 40$ kg
Suspension	$k_s = 2e4$ Nm^{-1}; $d_s = 2e3$ Nsm^{-1}
Tyre	$k_t = 2e5$ Nm^{-1}

In MATLAB we create a state-space model by entering the four matrices **A**, **B**, **C** and **D** and additionally use the command `sys`. To define the quarter car vehicle model in MATLAB the following lines have to be entered:

```
% Quarter Car Vehicle Model Parameters
ms  = 400;          % sprung mass [kg]
ma  =  40;          % unsprung mass [kg]
kt  = 2e5;          % tyre vertical stiffness [N/m]
ks  = 2e4;          % suspension vertical stiffness [N/m]
ds  = 2e3;          % suspension damping [Ns/m]

% State-space matrices
A = [-ds/ms  ds/ms  -ks/ms  ks/ms;
     ds/ma  -ds/ma  ks/ma  -(ks+kt)/ma;
     1  0  0  0;
     0  1  0  0];
B = [0; kt/ma; 0; 0];
C = [-ds/ms  ds/ms  -ks/ms  ks/ms;
     0  0  0  -kt;
     0  0  -1  1;
     0  0  1  0;
     0  0  0  1];
D = [0; kt; 0; 0; 0];

% State-space system definition
sys = ss(A,B,C,D);
```

---

the transfer function equals 1 and the phase angle equals 0 deg. At approximately 1 Hz, a resonance peak is observed in the transfer function of the sprung mass. At this frequency, the sprung mass is resonating on the suspension and the road inputs are amplified. The amplitude ratio of this peak is very sensitive to the damping level. On typical passenger cars, this ratio will be in the range of 1.5 to 3 [3]. For frequencies higher than this resonance frequency, the road inputs are increasingly attenuated. At approximately 10 Hz, the unsprung mass goes into a vertical resonance (wheel hop). This resonance causes also a small bump in the transfer function of the sprung mass.
The damped (ω_d) and undamped (ω_n) natural frequencies and damping ratios (ζ) of the system are calculated from the eigenvalues of the system matrix **A**. The eigenvalues are the values of λ for which:

$$|\lambda \mathbf{I} - \mathbf{A}| = 0 \tag{2.30}$$

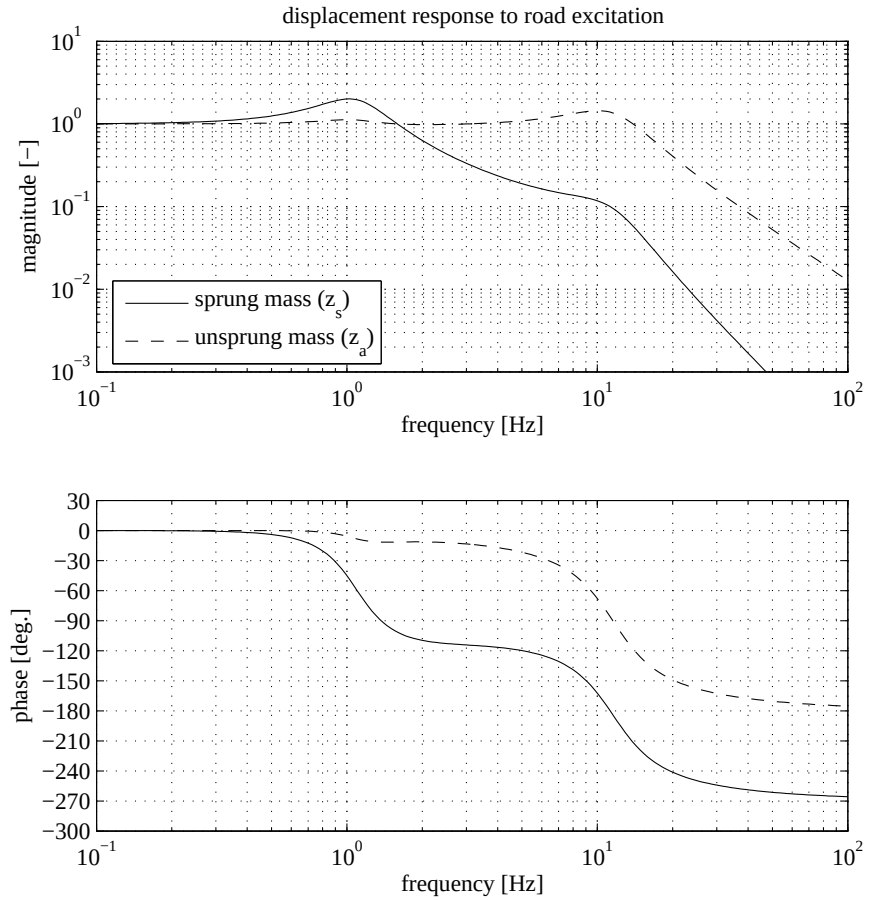

Figure 2.3: Transfer functions of the displacement responses to road excitation

Because the coefficients of the characteristic equation that results from equation (2.30) are real, a complex eigenvalue must occur in a complex conjugate pair:

$$\lambda_{1,2} = a \pm ib \tag{2.31}$$

In figure 2.4 the geometric relations between the characteristic values (or eigenvalues) and ω_d, ω_n and ζ are illustrated.
Consequently, the damped (f_d) and undamped (f_n) natural frequencies in Hz and damping ratio (ζ) of the system can be obtained from the complex eigenvalues as follows:

$$f_d = \frac{b}{2\pi} \tag{2.32}$$

$$f_n = \frac{|\lambda|}{2\pi} = \frac{\sqrt{a^2 + b^2}}{2\pi} \tag{2.33}$$

$$\zeta = -\frac{a}{|\lambda|} \tag{2.34}$$

For good ride, the damping ratio on modern passenger cars usually falls between 0.2 (20%) and 0.4 (40%) [3]. Because of the way damping influences the resonant frequency (see figure 2.4), the undamped and damped natural frequencies are usually quite close. With

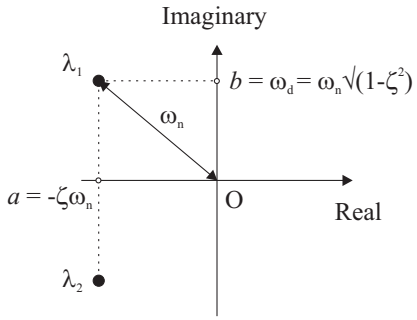

Figure 2.4: Eigenvalue location in terms of damped (ω_d) and undamped (ω_n) natural frequencies and damping ratio (ζ)

In Matlab the following lines can be used to generate the plots of the transfer functions:

```
freq = logspace(-1,2,200);      % frequency vector [Hz]

[mag,phase] = bode(sys,freq*2*pi);

subplot(2,1,1)
loglog(freq,squeeze(mag(4,1,:)),'k',freq,squeeze(mag(5,1,:)),'k--')
axis([0.1 100 1e-3 10])
xlabel('frequency [Hz]'); ylabel('magnitude [-]')
title('displacement response to road excitation')
legend('sprung mass (z_s)','unsprung mass (z_a)',3)

subplot(2,1,2)
semilogx(freq,squeeze(phase(4,1,:)),'k',freq,squeeze(phase(5,1,:)),'k--')
axis([0.1 100 -300 30])
xlabel('frequency [Hz]'); ylabel('phase [deg.]')
```

Note that the command `squeeze` is used to remove the singleton dimensions. Furthermore, note that `mag` and `phase` are arrays of size [(number of outputs) (number of inputs) (length of `freq`)]. For more information use the `MATLAB help` command.

---

a damping ratio of 0.2, the damped natural frequency is 98% of the undamped natural frequency, and even at a damping ratio of 0.4, it is about 92%. Because there is so little difference, the undamped natural frequency is commonly used to characterize the vehicle. The natural frequencies and damping ratios of our quarter car vehicle model equal:

- $f_n = 1.10$ Hz; $f_d = 1.04$ Hz; $\zeta = 31\%$, bounce
- $f_n = 11.6$ Hz; $f_d = 10.8$ Hz; $\zeta = 35\%$, wheel hop

Neglecting the influence of damping, both resonances can be approximated by the systems depicted in figure 2.5. The bounce resonance may be approximated by the sprung mass vibrating on the suspension and tyre springs in series. The wheel hop resonance can be approximated by the sprung mass vibrating on the suspension and tyre stiffnesses in parallel.

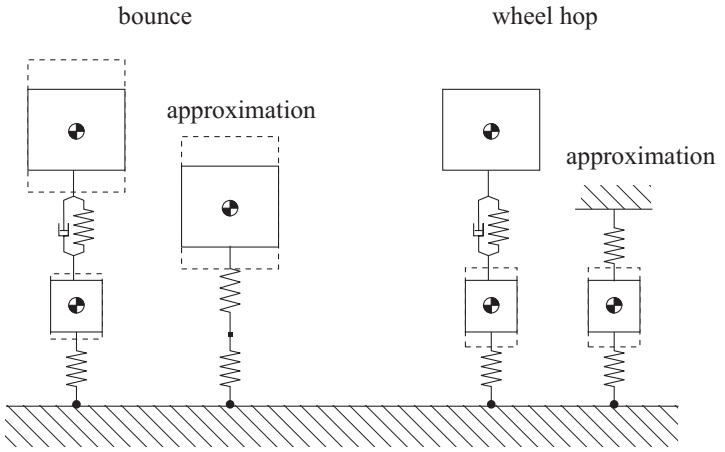

Figure 2.5: Approximations for the bounce and wheel hop mode

In MATLAB two commands can be used to calculate the natural frequencies and damping ratios: `eig` and `damp`.

Using `eig`:

```
ev = eig(sys);           % Calculates eigenvalues
fn = abs(ev)/(2*pi);     % Undamped natural frequencies [Hz]
Z = -real(ev)./abs(ev); % Damping ratios [-]
fd = fn.*sqrt(1-Z.^2);  % Damped natural frequencies [Hz]
```

Using `damp`:

```
[Wn,Z] = damp(sys);      % Undamped natural frequencies [Hz]
                         % + damping ratios [-]
fn = Wn/(2*pi);          % Undamped natural frequencies [Hz]
fd = fn.*sqrt(1-Z.^2);  % Damped natural frequencies [Hz]
```

In MATLAB the step response of a linear system can be calculated with the `step` command.

```
time = [0:0.005:2];      % time vector [s]
y = step(sys,time);      % calculating step response
y = y*0.01;              % scale the output for a step of 0.01 m
```

Note that MATLAB calculates the step response for a unit input, i.e. in our case for a step in road profile of 1 m. Since we have a linear system, we may scale the output with a factor 0.01 to obtain the step response for 10 mm. It must be remarked that for more general input signals the command `lsim` can be used. See MATLAB help for more details. Further, note that $\mathbf{y}$ is a matrix that has the following dimensions: (number of data points of the time vector) x (number of outputs of the system).

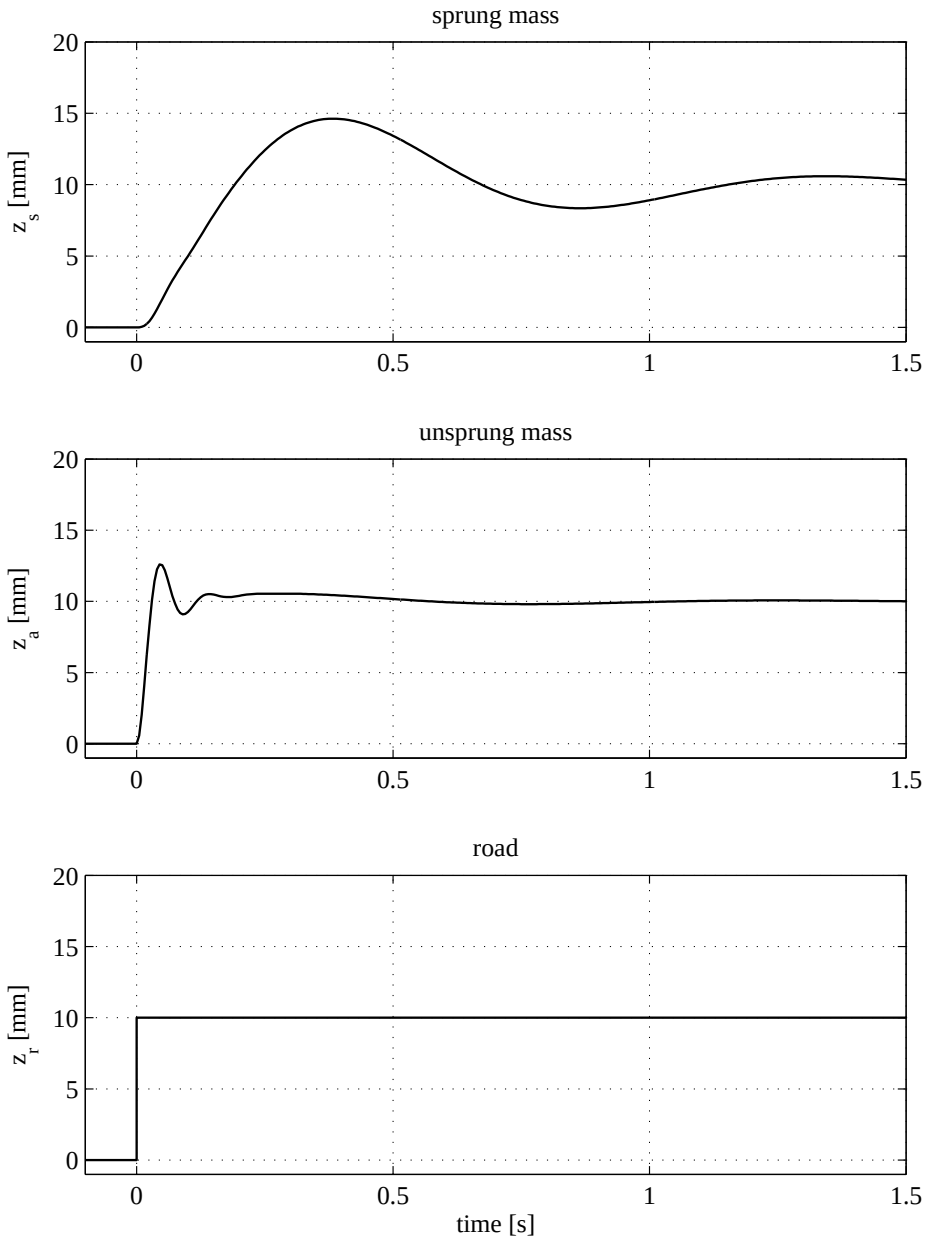

Figure 2.6: Quarter car vehicle model response to a 10 mm step in road profile

In figures 2.6 and 2.7 the time responses of our quarter car vehicle model are plotted for driving over a 10 mm step in road profile. In these responses the two resonances of the system (bounce and wheel hop) can be clearly observed.

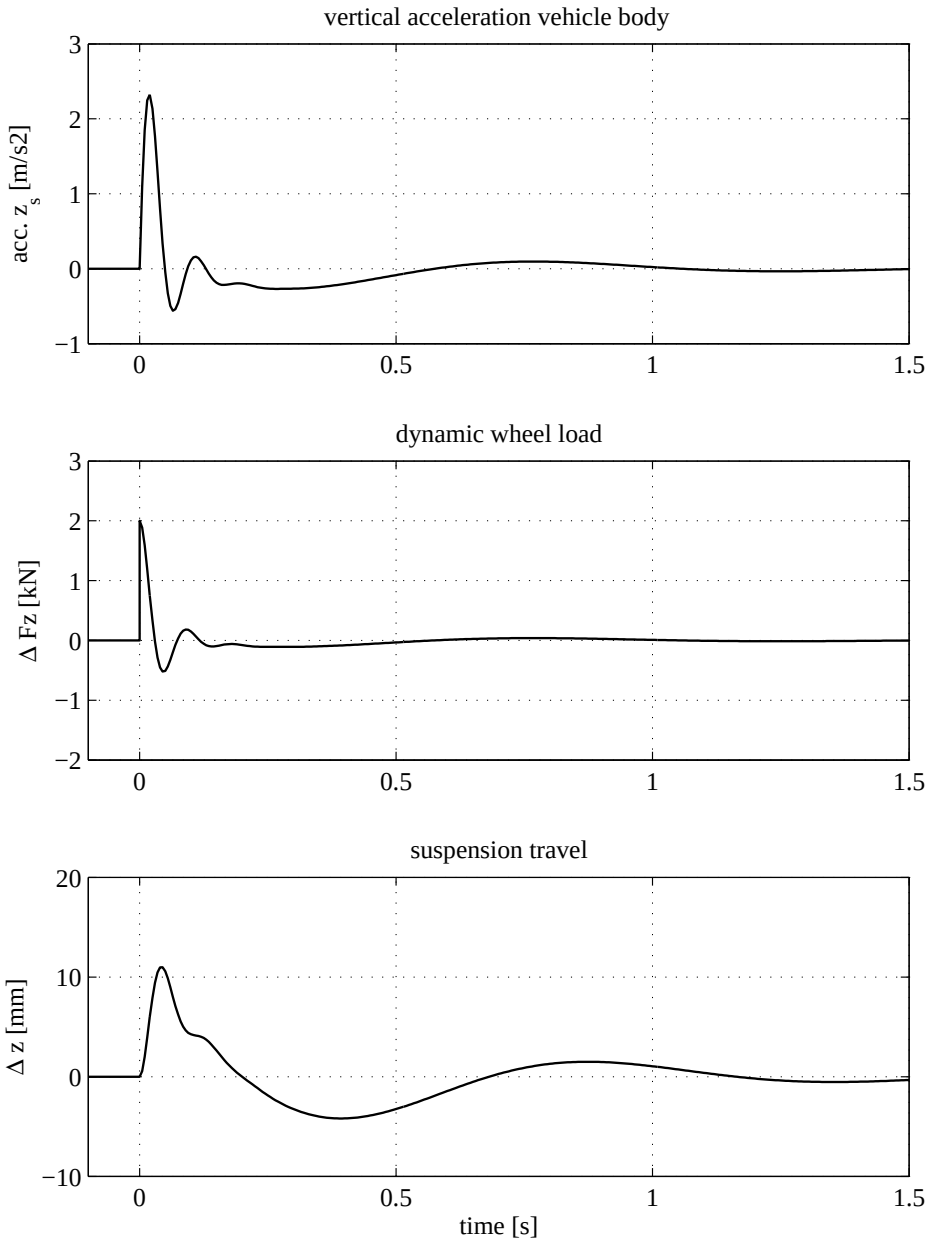

Figure 2.7: Quarter car vehicle model response to a 10 mm step in road profile

2.3 Analysis in the frequency domain

In the previous section, the vehicle response on a step in road profile has been studied. During normal driving however, road profiles are rarely of simple forms. In practice, road profiles encompass every form of roughness from potholes resulting from localized pavement failures to the ever-present random deviations reflecting the practical limits of precision to which the road surface can be constructed and maintained. Therefore, road profiles fit the general category of 'broad band random signals'. Hence, they can

be described either by the profile itself or by its statistical properties. Hereafter, some of these statistical properties will be discussed.

The mean value m or expected value E of a random signal $x(t)$ in the time interval 0 to T is defined as:

$$m = \frac{1}{T}\int_0^T x(t)dt = E[x(t)] \tag{2.35}$$

The mean square value (MSV) is defined as:

$$\text{MSV} = \frac{1}{T}\int_0^T x(t)^2 dt = E[x(t)^2] \tag{2.36}$$

The variance σ^2 or standard deviation σ is defined as:

$$\sigma^2 = \frac{1}{T}\int_0^T (x(t) - m)^2 dt = E[(x(t) - E[x(t)])^2] \tag{2.37}$$

Consequently, the relation between these properties is:

$$\sigma^2 = \text{MSV} - m^2 \tag{2.38}$$

Notice that if the expected value ($m = 0$) equals zero, the root mean square value (RMS) equals the standard deviation:

$$\text{RMS} = \sqrt{\text{MSV}} = \sigma \qquad \text{if} \quad m = 0 \tag{2.39}$$

As an example, figure 2.8 presents the amplitude content of a typical road profile. Besides a plot of the amplitudes, the probability density function is plotted. In this plot the normal or Gaussian probability density function p is plotted as well. This function equals:

$$p(x) = \frac{1}{\sigma\sqrt{2\pi}} e^{-(x-m)^2/(2\sigma^2)} \tag{2.40}$$

It can be observed that for this road profile, the normal distribution fits well.

In MATLAB the previous statistical properties can be calculated as follows:

- mean: `m = mean(x);`
- mean square value: `MSV = var(x)+m.^2;`
- variance: `sigma2 = var(x);`
- standard deviation: `sigma = std(x);`
- normal probability density function: `p = normpdf(x,m,sigma);`

The autocorrelation function R_x is defined as:

$$R_x(\tau) = \frac{1}{T}\int_0^T x(t)x(t+\tau)dt = E[x(t)x(t+\tau)] \tag{2.41}$$

in which τ is a time shift. Notice that:

$$R_x(\tau = 0) = E[x(t)^2] = \text{MSV} \tag{2.42}$$

The spectral density S_x is the Fourier transform of the autocorrelation function:

$$S_x(\omega) = \frac{1}{2\pi} \int_{-\infty}^{\infty} R_x(\tau) e^{-i\omega\tau} d\tau \tag{2.43}$$

Conversely, the autocorrelation function can be obtained by an inverse Fourier transform of the spectral density:

$$R_x(\tau) = \int_{-\infty}^{\infty} S_x(\omega) e^{i\omega\tau} d\omega \tag{2.44}$$

For $\tau = 0$ we find:

$$R_x(\tau = 0) = \int_{-\infty}^{\infty} S_x(\omega) d\omega \tag{2.45}$$

Consequently, by integrating the spectral density function we can obtain the mean square value (compare equations (2.42) and (2.45))! If the mean value equals zero ($m = 0$), which is often the case for road profiles, we can directly obtain the standard deviation (see equation (2.38)). For more information on random processes it is referred to [5].

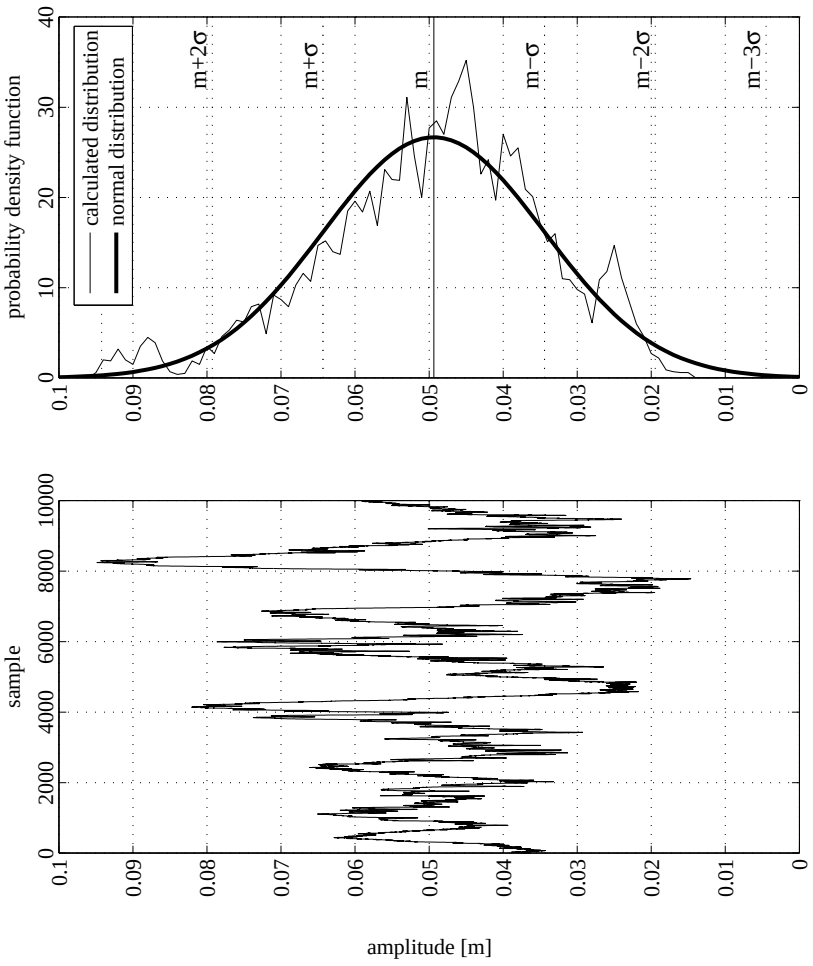

Figure 2.8: Example of the amplitude content of a road surface

2.4 Transmission of random vibrations

Consider a dynamic system with input $x(t)$ and output $y(t)$. The relation between the input and output is described by the transfer function H_{xy}:

$$y(\omega) = H_{xy}(\omega)x(\omega) \tag{2.46}$$

For random signals, like road profiles, it is more convenient to use the power spectral density $S_x(\omega)$ of the signal $x(t)$ as input. In that case, the output is the power spectral density $S_v(\omega)$ of $y(t)$. It can be shown that in this case we have to use the squared value of the absolute value of the (complex) transfer function H_{xy}:

$$S_y(\omega) = |H_{xy}(\omega)|^2 S_x(\omega) \tag{2.47}$$

Both relations are shown schematically in figure 2.9. Considering our quarter car vehicle model again, the input signal $x(t)$ is the road profile height and the output signals are for example the vertical acceleration of the body, the dynamic tyre force and the suspension travel.

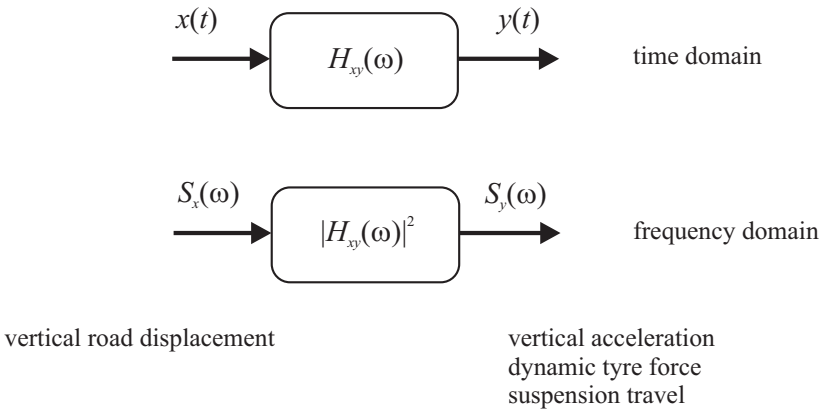

Figure 2.9: Relation between transfer functions, signals and power spectral densities

2.5 Random road profiles

As mentioned before, in practice road profiles are random signals. As an example, figure 2.10 presents a road profile of 1000 m for the left and right track of a vehicle, measured with a sample interval of 0.05 m. In the upper plot, the complete road profiles and in the lower plot a 10 m section of the road profiles are plotted. It can be observed that low frequency unevenness has large amplitudes, whereas high frequency unevenness has small amplitudes.

It is common to represent a road profile by its displacement power spectral density (PSD). In figure 2.11 the power spectral densities of the measured road profiles are plotted. In addition, the ISO road class limits A-H are shown [1]. The spatial frequency n is defined by the relation:

$$n = \frac{1}{\lambda} = \frac{f}{V} \tag{2.48}$$

where λ is the road surface wavelength, f the frequency and V the vehicle forward velocity.

Measurements on various road types have revealed that a slope of about '-2' on a log-log scale appears for many road surfaces. In addition, it has been found that different

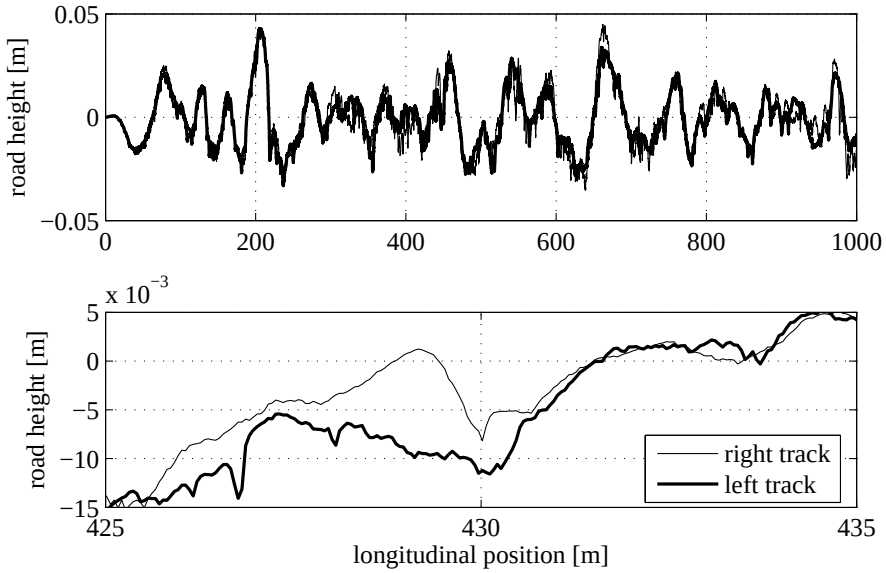

Figure 2.10: Measured road profiles for the left and right tracks of a vehicle

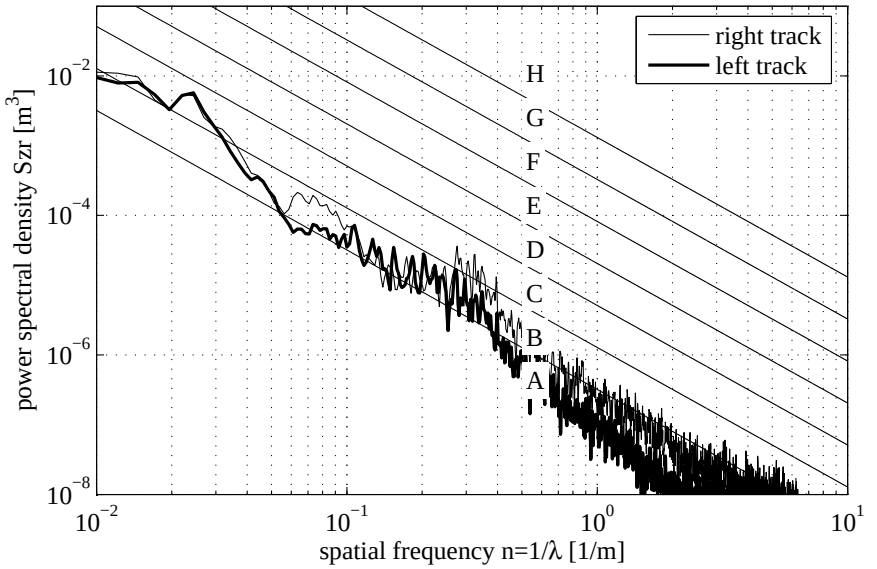

Figure 2.11: Displacement power spectral densities of the measured road profiles and road classification limits according to ISO 8608:1995(E)

road surface types (smooth asphalt, Belgian blocks, etc.) will mainly result in a vertical shift of the PSD. Therefore, in [1] the following expression is proposed to represent a road profile:

$$S_{zr}(n) = S_{zr}(n_0)\left(\frac{n}{n_0}\right)^{-2} \qquad \text{with:} \quad n_0 = 0.1 \text{ m}^{-1} \tag{2.49}$$

Closely related to this relation are the road classes A-H. Table 2.2 presents the values that belong to the class limits. For simulation purposes, the mean values may be used. Finally,

notice that this 'spatial' frequency domain PSD only considers geometrical road surface data. When performing simulations it is often convenient to use the 'time' frequency

Table 2.2: Classification of road roughness according to ISO 8608:1995(E)

	degree of roughness $S_{zr}(n_0)$, 10^{-6} m^3	
Road class	upper limit	geometric mean
A (very good)	32	16
B (good)	128	64
C (average)	512	256
D (poor)	2048	1024
E (very poor)	8192	4096
F	32768	16384
G	131072	65536
H	-	262144

domain PSD $S_{zr,f}$ instead of the displacement PSD S_{zr} (spatial frequency domain). The relation between these two PSDs can be derived as follows: The variance/standard deviation of the road amplitude will be the same in the distance and time domain. Hence, if $m = 0$:

$$\begin{aligned} \sigma_{zr}^2 &= E(z_r^2) \\ &= \int_{n=-\infty}^{n=\infty} S_{zr}(n)dn \\ &= \int_{f=-\infty}^{f=\infty} S_{zr,f}(f)df \end{aligned} \tag{2.50}$$

Substitution of equation (2.48) into equation (2.56) gives:

$$\int_{f=-\infty}^{f=\infty} S_{zr}\left(\frac{f}{V}\right)\frac{1}{V}df = \int_{f=-\infty}^{f=\infty} S_{zr,f}(f)df \tag{2.51}$$

Thus for a constant velocity V we may write:

$$S_{zr,f}(f) = \frac{1}{V}S_{zr}\left(\frac{f}{V}\right) \tag{2.52}$$

As an example, figure 2.12 presents 'time' frequency domain PSDs for 30 and 120 kmh^{-1}. When considering the transfer functions of the quarter car vehicle model (figure 2.3), it is clear that the natural frequencies of the system will be excited more for a velocity of 120 kmh^{-1} than for 30 kmh^{-1}.

2.6 Ride comfort

Due to its subjective nature ride comfort is difficult to assess. Nevertheless, many recent research results show a minimum tolerance (maximum sensitivity) of the human body to vertical vibrations in the frequency range between 4 and 8 Hz. This sensitivity is the result of vertical resonances of the abdominal cavity. See figure 2.13, where the human body is depicted as a multibody system. At frequencies above and below this range, the tolerance increases in proportion to frequency. The sensitivity to horizontal vibrations is somewhat different from that of vertical. The most remarkable difference is that the region of maximum sensitivity occurs in the 0.5 to 2 Hz range. In fore/aft direction, this sensitivity is generally recognized to result from the fore/aft resonance of the upper torso.

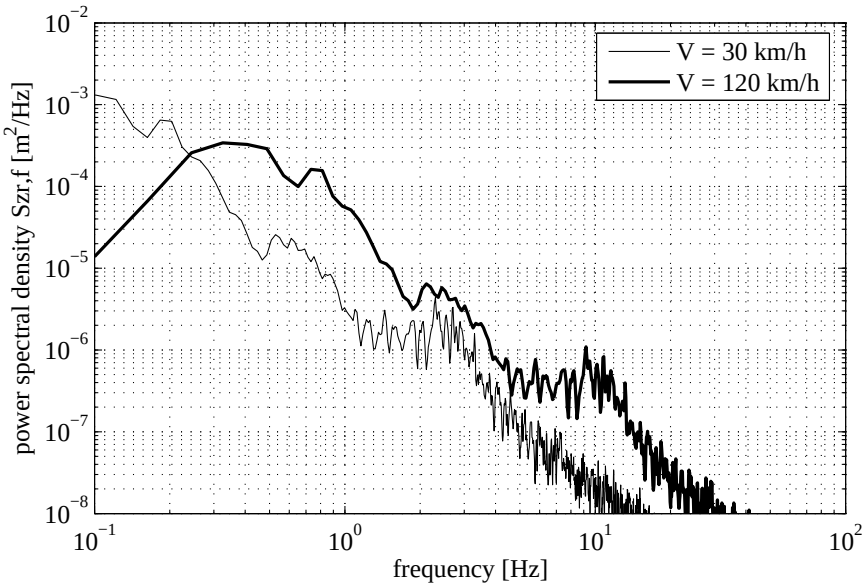

Figure 2.12: 'Time' frequency domain PSDs of the measured road profiles

---

In Matlab the power spectral density can be estimated with the command `pwelch`. The following lines can be used to generate a plot of the displacement PSD of a road surface:

```
load roaddata           % load road data file
xroad = road(:,1);      % longitudinal position [m]
zroad = road(:,2);      % road height [m]
dx = xroad(2)-road(1);  % road sample interval [m]

[Szr,n] = pwelch(zroad,[],[],[],1/dx); % PSD estimate

loglog(n,Szr); grid;
xlabel('spatial frequency n=1/\lambda [1/m]');
ylabel('power spectral density Szr [m^3]');
```

The variance can be estimated by calculating the area under the PSD:

```
var_estimate = sum(Szr)*(n(2)-n(1));
```

Finally, be careful with other commands like `psd` and `spectrum` to obtain the PSD estimate!

According to [2] ride comfort is assessed in the 0.5 to 80 Hz range. Above 80 Hz, the human body is not very sensitive to vibrations. In the 0.1 to 0.5 Hz range, vibrations may cause motion sickness. To account for the human body sensitivity for specific frequencies, weighting functions $H_{iso}(f)$ are applied to the vertical, longitudinal and lateral acceleration signals. As shown in figure 2.14, weighting functions are defined for the vertical and

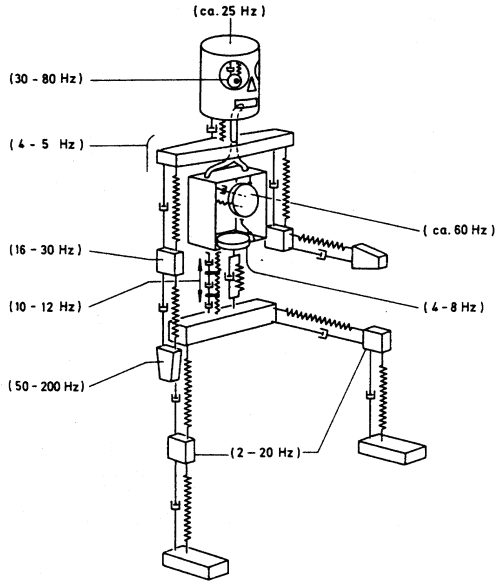

Figure 2.13: The human body depicted as a multibody system [6]

horizontal directions. In addition, a weighting function is defined for assessing motion sickness (only vertical direction).

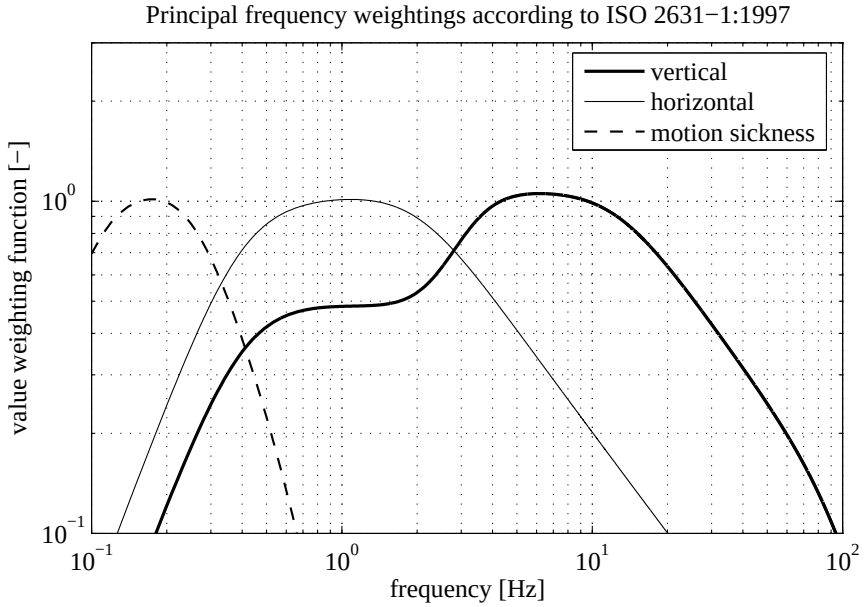

Figure 2.14: Acceleration weighting functions according to [ISO 2631-1, 1997]

By applying the weighting function for the vertical direction, the frequency-weighted vertical acceleration of the sprung mass $\ddot{z}_{s,iso}$ is obtained as follows:

$$\ddot{z}_{s,iso}(f) = H_{iso,z}(f)\ddot{z}_s(f) \tag{2.53}$$

In terms of power spectral densities, this equation reads:

$$S_{\ddot{z},iso}(f) = |H_{iso,z}(f)|^2 S_{\ddot{z}}(f) \tag{2.54}$$

For vibrations in more than one direction, the vibration total value of weighted RMS acceleration a_v, determined from vibration in orthogonal coordinates is calculated as follows:

$$a_v = \sqrt{k_x^2 a_{wx}^2 + k_y^2 a_{wy}^2 + k_z^2 a_{wz}^2} \tag{2.55}$$

where:

- a_{wx}, a_{wy} and a_{wz} are the weighted RMS accelerations with respect to the orthogonal axes x (longitudinal), y (lateral), z (vertical), respectively
- k_x, k_y and k_z are multiplying factors

For assessing comfort of seated persons, the factors k_x, k_y and k_z equal 1. According to [2] it is recommended to use the ***vibration total value*** a_v for assessing comfort. Note that the weighted acceleration values can be obtained by calculating the areas under the corresponding weighted power spectral densities. Acceptable values of vibration magnitude for comfort depend on many factors. Therefore a limit is not defined in [2]. Nevertheless, the values in table 2.3 give approximate indications of likely reactions to various magnitudes of overall vibration total values in public transport. From now on, we

Table 2.3: Comfort reactions to vibration environment in public transport according to ISO 2631-1:1997(E)

vibration total value	likely reaction
< 0.315 ms^{-2}	not uncomfortable
0.315 ms^{-2} to 0.63 ms^{-2}	a little uncomfortable
0.5 ms^{-2} to 1 ms^{-2}	fairly uncomfortable
0.8 ms^{-2} to 1.6 ms^{-2}	uncomfortable
1.25 ms^{-2} to 2.5 ms^{-2}	very uncomfortable
> 2 ms^{-2}	extremely uncomfortable

call the vibration total value the ***ride comfort index***. Notice that for vibration in only one direction, the ride comfort index equals the RMS value obtained from the weighted acceleration power spectral density.

As an example we consider the quarter car vehicle model driving with a velocity of 20 ms^{-1} (72 kmh^{-1}) over a poor road surface (ISO road class D). The PSD of the road surface is obtained by using equations (2.49) and (2.52) and table 2.2:

$$S_{zr,f}(f) = S_z r(n_0) \frac{1}{V} \left(\frac{f}{V n_0} \right)^{-2} = 1024 \cdot 10^{-6} V \left(\frac{f}{0.1} \right)^{-2} \tag{2.56}$$

The power spectral densities of the vehicle responses are calculated by using equation (2.47). For obtaining the ride comfort index, the power spectral density of the vertical acceleration of the sprung mass is weighted according to equation (2.54). In figures 2.15, 2.16 and 2.17, it is illustrated how the responses are calculated for the vertical acceleration of the body, the dynamic wheel loads and the suspension travel, respectively. In these figures, the power spectral densities and response gains are plotted in the frequency range 0.1-50 Hz.

By calculating the areas under the power spectral densities, the mean square values of the response signals can be estimated. Table 2.4 presents the RMS values that are obtained from the mean square values. If normal distributions are assumed, it is expected that the peak values of the responses, which occur while driving over this road surface, will

Table 2.4: RMS and peak values of the calculated responses

parameter	RMS value	peak value (3*RMS)
vertical acceleration	2.48 ms^{-2}	7.44 ms^{-2}
comfort index	2.11 ms^{-2}	6.34 ms^{-2}
dynamic wheel load	1512 N	4535 N
suspension travel	21 mm	63 mm

be roughly 3 times the RMS values (compare figure 2.8). These peak values are important for designing a suspension system. For example, the space required to accommodate the dynamic axle motion is at least 127 mm. Finally, note that with our simple road description (equation (2.56)), the RMS values depend on the square root of the forward velocity. Thus: the higher the velocity, the worse the comfort.

2.7 Optimization of the suspension

In this section, on the basis of an example, it is discussed how the suspension system can be optimized in order to comply with certain design requirements. These design requirements are:

- improve ride comfort, i.e. minimize the ride comfort index
- minimize dynamic wheel load fluctuations (important for road holding)
- keep suspension travel within feasible limits

If we consider our quarter car vehicle model, it is easy to see that the following parameters might be optimized to comply as good as possible with the design requirements:

- damping constant d_s
- vertical suspension stiffness k_s
- unsprung mass m_a (limited)
- tyre vertical stiffness k_t (very limited)

To investigate the influence of the different parameters on the design requirements, the quarter car vehicle model driving with 20 ms^{-1} over the road surface defined in the previous section is used.

First, we start with varying the damping constant and we keep the other parameters constant. In figure 2.18 the relevant design parameters are plotted. As can be observed from the figure, there is no overall optimum. The optimal damping for comfort is 559 $Ns.m^{-1}$, whereas the optimal damping for minimizing the dynamic tyre loads is 2477 $Ns.m^{-1}$. For minimizing the suspension travel, the damping constant must be as high as possible. Thus, a compromise has to be made. Table 2.5 presents the numerical values for the two minima found.
In figure 2.19 the transfer functions of the vertical acceleration response and dynamic tyre load response to road excitation are compared for the two optimal damping values. As can be observed, the transfer functions for maximum comfort show a dip in the frequency range where the ISO weighting curve (figure 2.14) shows a maximum, which implies that the area under the final PSD of the weighted acceleration is minimal. The transfer functions for

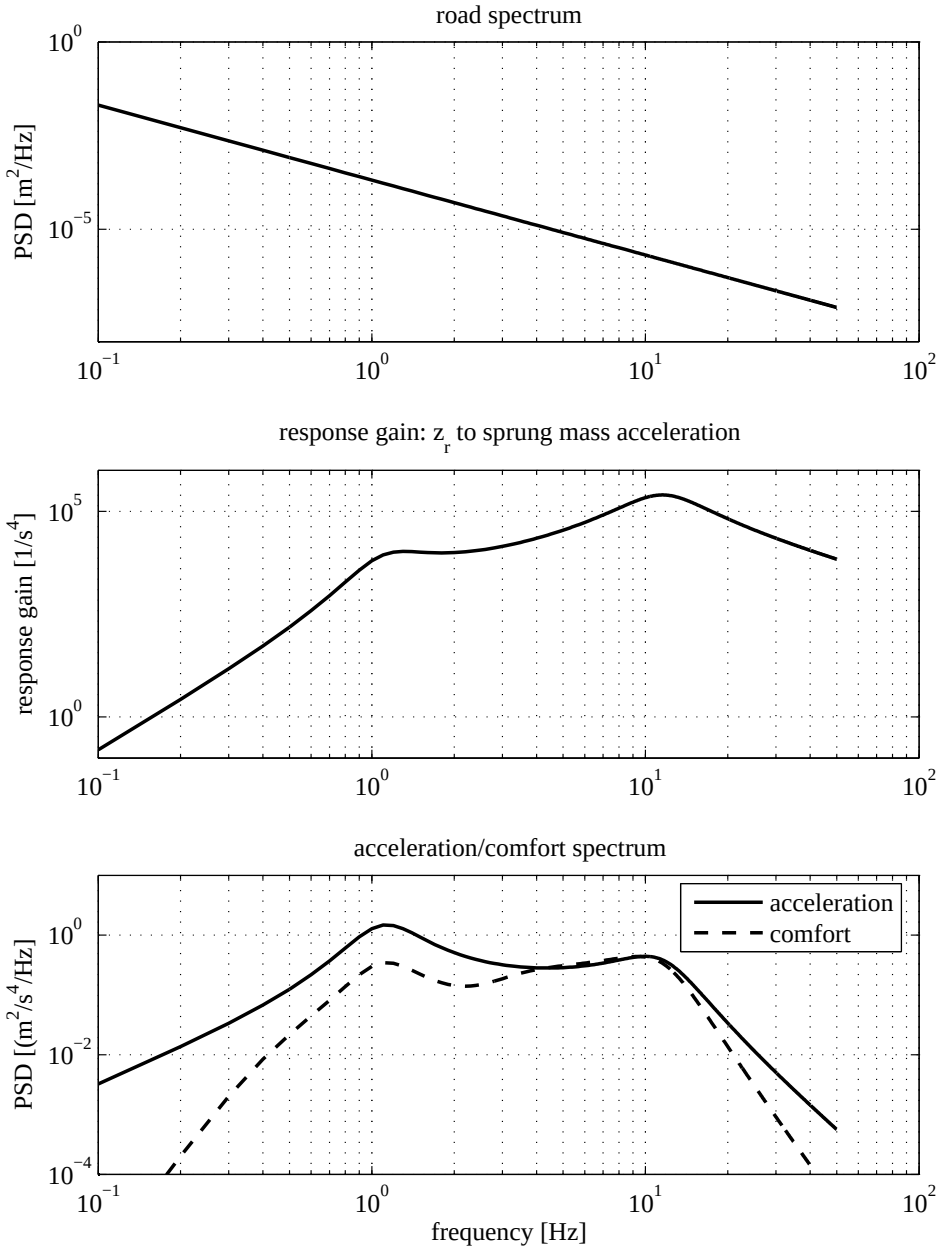

Figure 2.15: Calculations of vehicle response for a forward velocity of 20 ms^{-1}: acceleration and comfort power spectral densities

minimizing the dynamic tyre loads do not show a clear dip, but show a higher magnitude for higher frequencies. Notice that in this case (no weighting function is applied) this is beneficial, because the overall area under the PSD of the dynamic tyre loads is of importance and the road surface PSD decreases with frequency.
The next step in our optimization process is to vary the vertical suspension stiffness. For each value of the stiffness, the optimal damping constant is obtained for both maximum comfort and minimum dynamic tyre loads. In figure 2.20, the various optimal combinations

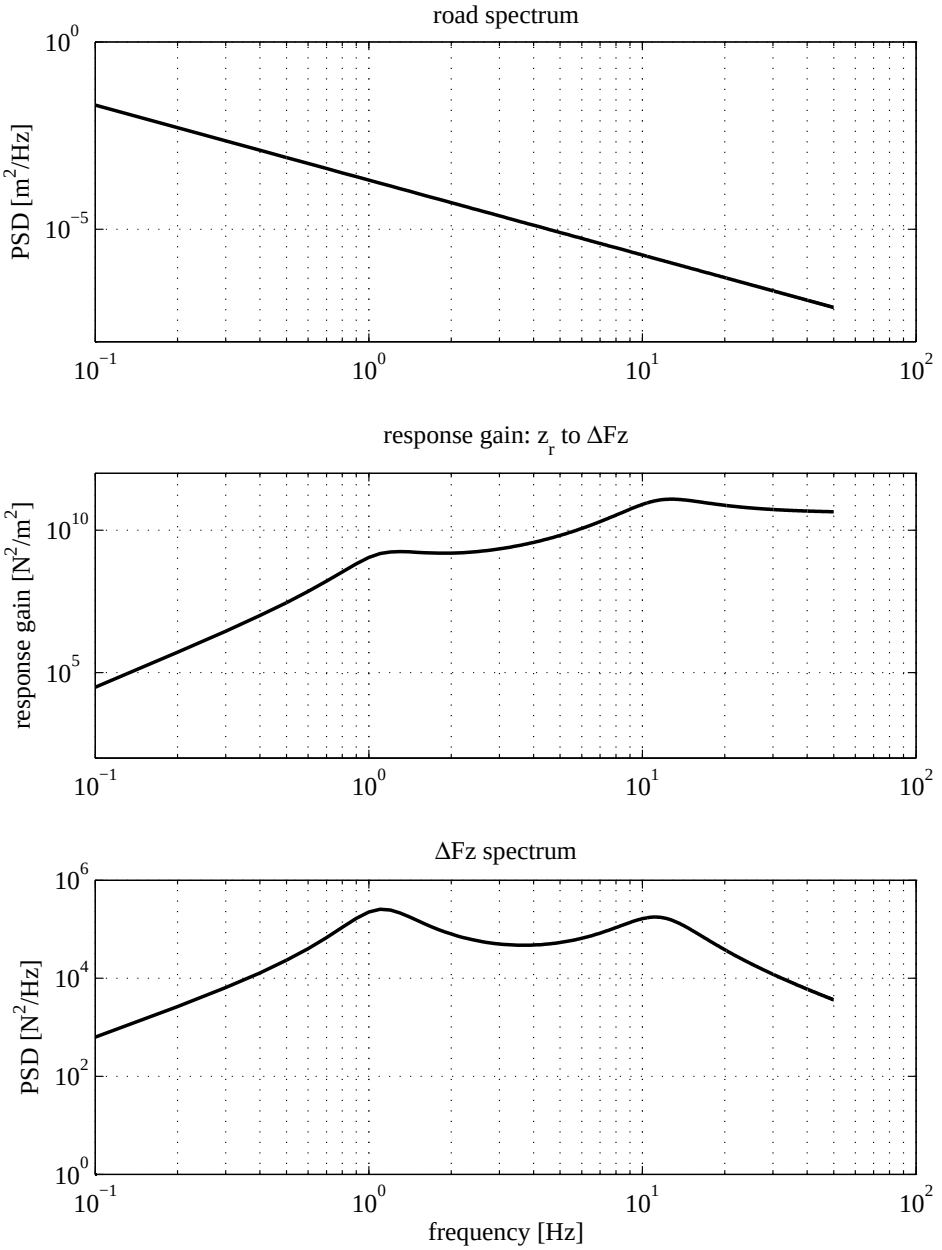

Figure 2.16: Calculations of vehicle response for a forward velocity of 20 ms^{-1}: dynamic wheel load power spectral density

are depicted. As can be observed, reducing the vertical stiffness can significantly improve ride comfort. The drawback however is that we then get an increase of spring travel and dynamic wheel loads. In case of conventional coil springs, a significant portion of the available spring travel is used to cope with static load variations due to for example the number of passengers and their luggage. Having a low spring stiffness would mean that we have to allow a very large spring travel, which is undesirable for packaging reasons, suspension kinematics, drive shafts, etc. In normal passenger cars, the available spring

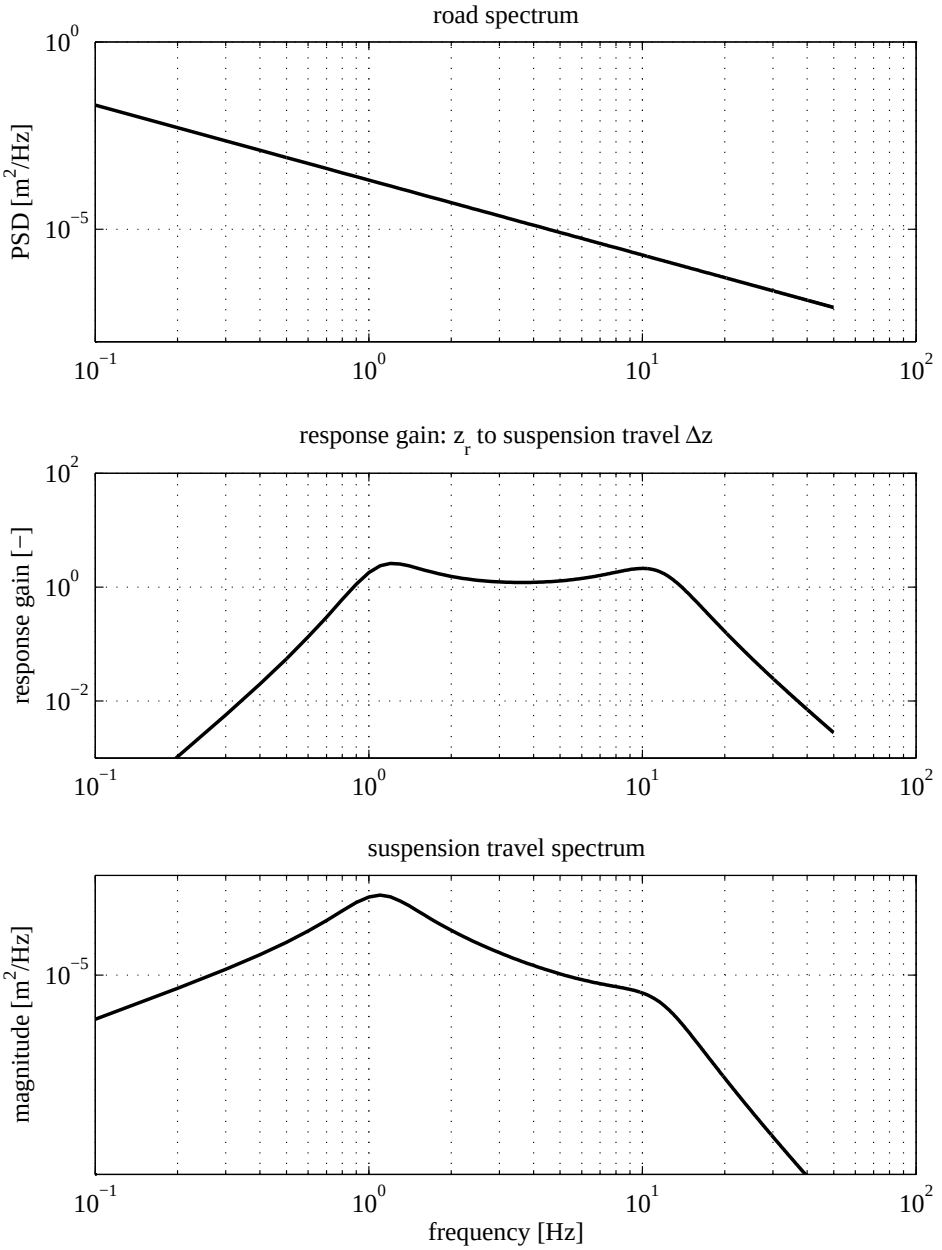

Figure 2.17: Calculations of vehicle response for a forward velocity of 20 ms^{-1}: suspension travel power spectral density

travel is therefore limited to about 150 mm. For example, a static wheel load variation of 100 kg and a vertical stiffness of 20 kNm^{-1} gives a suspension travel of 50 mm. Assuming a total travel of 150 mm and a static travel at kerb height of 75 mm, this reduces the available dynamic travel of the wheel in upward direction to only 25 mm. Conversely, on vehicles equipped with hydropneumatic or air suspension systems, lower vertical stiffnesses can be used, because these suspension systems can compensate for static load variations.

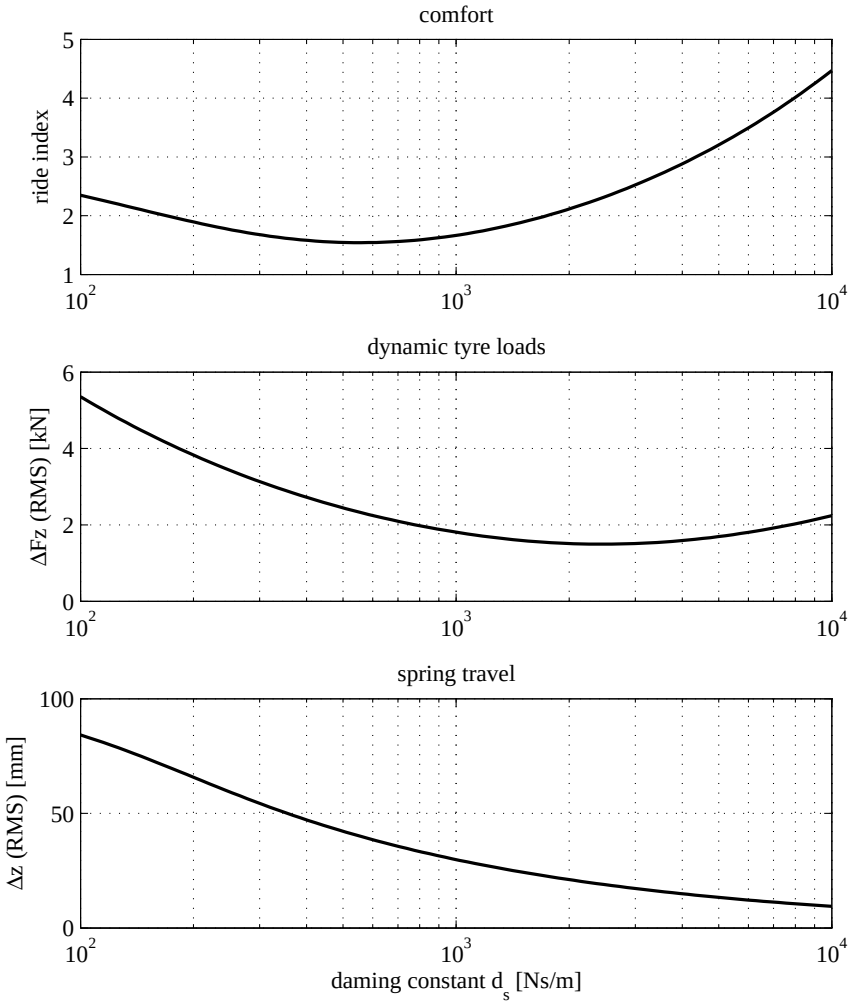

Figure 2.18: Influence of damping constant on relevant design parameters

Reducing the unsprung mass will both improve ride comfort and reduce dynamic tyre loads. The effect of reducing the unsprung mass will be illustrated with an example. In the example, 10 kg of the unsprung mass of our original quarter car vehicle model is moved to the sprung mass. As can be seen in table 2.6, the ride comfort index and the dynamic wheel loads are reduced.
The dynamic tyre loads can also be reduced significantly by lowering the tyre vertical stiffness. The example in table 2.7 illustrates this. The drawback of lowering the tyre vertical stiffness is that it can only be achieved by reducing the tyre pressure, which may adversely affect other important characteristics (e.g. vehicle handling, tyre wear, rolling resistance). Therefore, the possibilities to reduce tyre pressure are very limited.

2.8 Possible improvements of the suspension system

In the previous section, the parameters of the quarter car vehicle model were optimized in order to comply with the design requirements. It was shown that no optimal setting could be obtained for all design requirements. Conversely, extreme settings were found that

Table 2.5: Design parameters for optimal damping values

design parameter	damping constant	
	$d_s = 559$ Nsm^{-1}	$d_s = 2477$ Nsm^{-1}
ride comfort index	1.54 ms^{-2}	2.32 ms^{-2}
dynamic wheel load (RMS)	2321 N	1495 N
suspension travel (RMS)	40 mm	19 mm

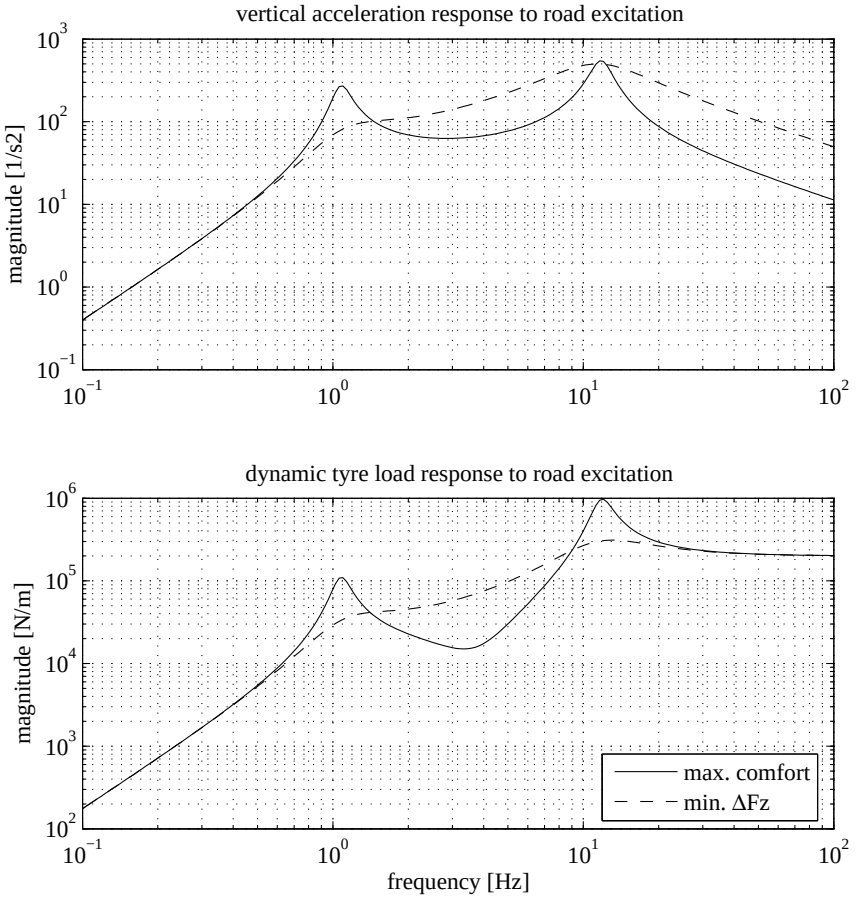

Figure 2.19: Influence of damping constants for maximum comfort and minimal dynamic tyre loads on the relevant transfer functions to road excitation

optimize the system either for optimal comfort or optimal road holding. In this section, two other possibilities to improve the suspension system will be given. These possibilities are:

- using a dynamic vibration absorber
- 'skyhook' damping

In the subsequent sections, these possibilities will be discussed in detail.

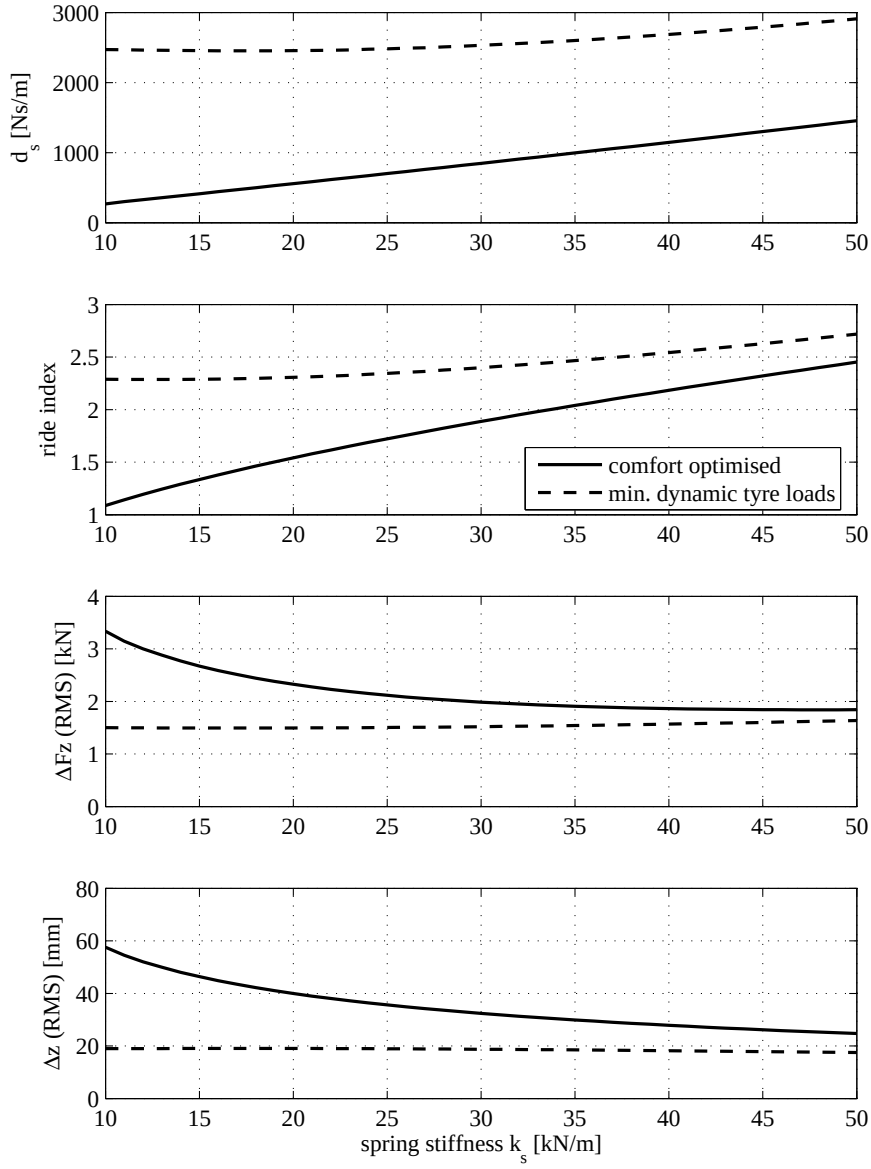

Figure 2.20: Optimal damping values for both maximum comfort and minimum dynamic tyre loads for various values of the spring stiffness k_s

Dynamic vibration absorber

A dynamic vibration absorber is an additional mass-spring system that is used to reduce the frequency response function of the combined system. For automotive vehicles, the additional mass can be the engine and gearbox. Figure 2.21 presents our quarter car vehicle model with the engine mass and mounts as a dynamic vibration absorber. As an example, we redistribute the sprung mass as follows: $m_s = 300$ kg, $m_e = 100$ kg. Next, the stiffness k_e and damping values de of the engine mounts are optimized in order to obtain the lowest ride comfort index. The upper plot of figure 2.22 presents the response

Table 2.6: Design parameters for the original and modified quarter car vehicle model showing the effect of moving 10 kg of mass from the unsprung mass to the sprung mass

	original	modified
ride comfort index	2.11 ms^{-2}	2.00 ms^{-2}
dynamic wheel load (RMS)	1512 N	1385 N
suspension travel (RMS)	21 mm	21 mm

Table 2.7: Design parameters for the original and modified quarter car vehicle model showing the effect of reducing the tyre vertical stiffness

	original	modified
vertical stiffness	200 Nmm^{-1}	150 Nmm^{-1}
ride comfort index	2.11 ms^{-2}	1.86 ms^{-2}
dynamic wheel load (RMS)	1512 N	1224 N
suspension travel (RMS)	21 mm	21 mm

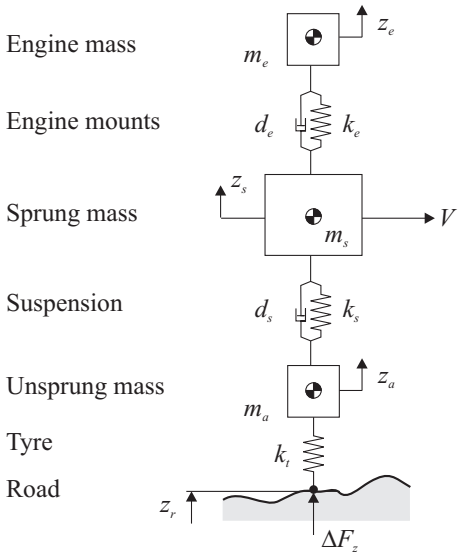

Figure 2.21: Quarter car vehicle model with the engine mass and mounts as dynamic vibration absorber

gains of the original and modified systems from the road profile height to the sprung mass acceleration. The lower plot shows the comfort spectrum. Again, the ISO class D road surface of equation (2.56) is used. The vehicle forward velocity is 20 ms^{-1}. In the plots, it can be observed that due to the introduction of the dynamic vibration absorber an extra resonance peak occurs at about 17 Hz. The dip in the response gain between this resonance peak and the wheel hop resonance at about 11 Hz finally leads to a reduction of the ride comfort index of 8.5%. In table 2.8 the results of the system with dynamic vibration absorber are compared with the results of the original system. Notice that the wheel loads and suspension travel remain unchanged. Finally, it must be noted that by introducing a dynamic vibration absorber an extra natural frequency is introduced, which may give rise to other problems. Therefore, careful tuning is required in practice.

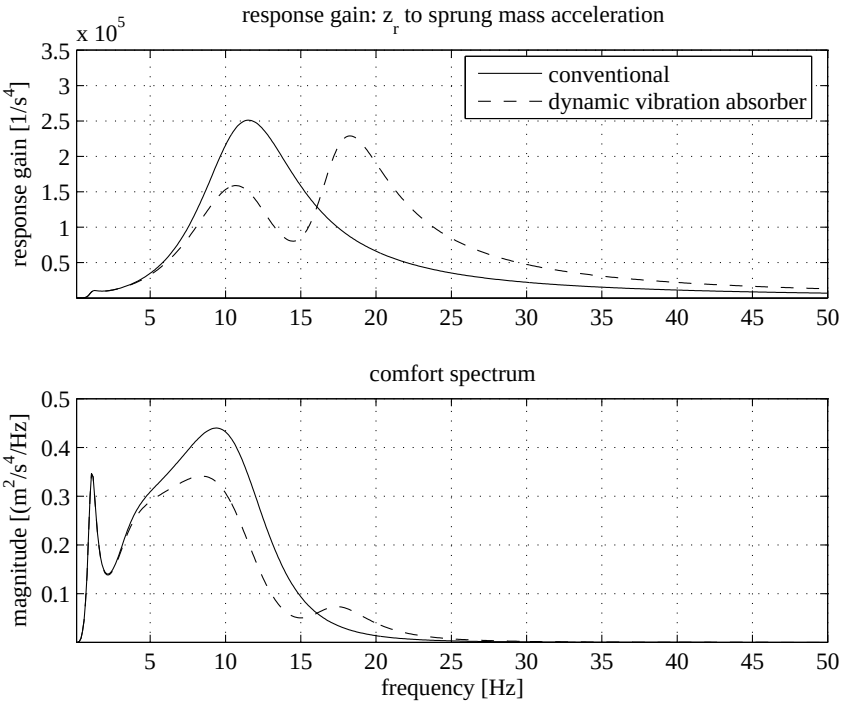

Figure 2.22: Response gain from road profile height to sprung mass acceleration and comfort spectrum for both a conventional system and one with a dynamic vibration absorber

Table 2.8: Design parameters for the original and modified quarter car vehicle model showing the effect of having a dynamic vibration absorber

	original	modified
ride comfort index	2.11 ms^{-2}	1.93 ms^{-2}
dynamic wheel load (RMS)	1512 N	1512 N
suspension travel (RMS)	21 mm	21 mm

'skyhook' damping

The theoretical principle of 'skyhook' damping is that a damper connects the sprung mass with a fixed point in the sky as illustrated in figure 2.23. As example, our quarter car vehicle model will be equipped with a 'skyhook' damper with a damping constant d_{sky} of 10000 Nsm^{-1}. In figure 2.24, the sprung mass displacement response to road excitations and the comfort spectrum of our modified system are compared with those of the original/conventional system. The ISO class D road surface of equation (2.56) is again used. The vehicle forward velocity is 20 ms^{-1}. It is observed that with a 'skyhook' damper it is possible to mainly eliminate the bounce resonance peak. In table 2.9, the design parameters of the system with the 'skyhook' damper are compared with those of the original quarter car system. It is shown that the ride comfort index decreases with about 17%, whereas the suspension travel increases with 30%. The dynamic wheel loads remain almost constant. In general, it can be said that increasing the skyhook damping constant always improves ride comfort. The problem however is how to realize a 'skyhook damper' in practice? This is the subject of the next section.

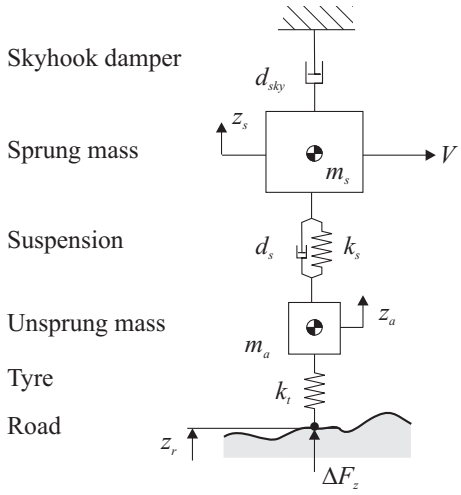

Figure 2.23: Theoretical principle of 'skyhook' damping

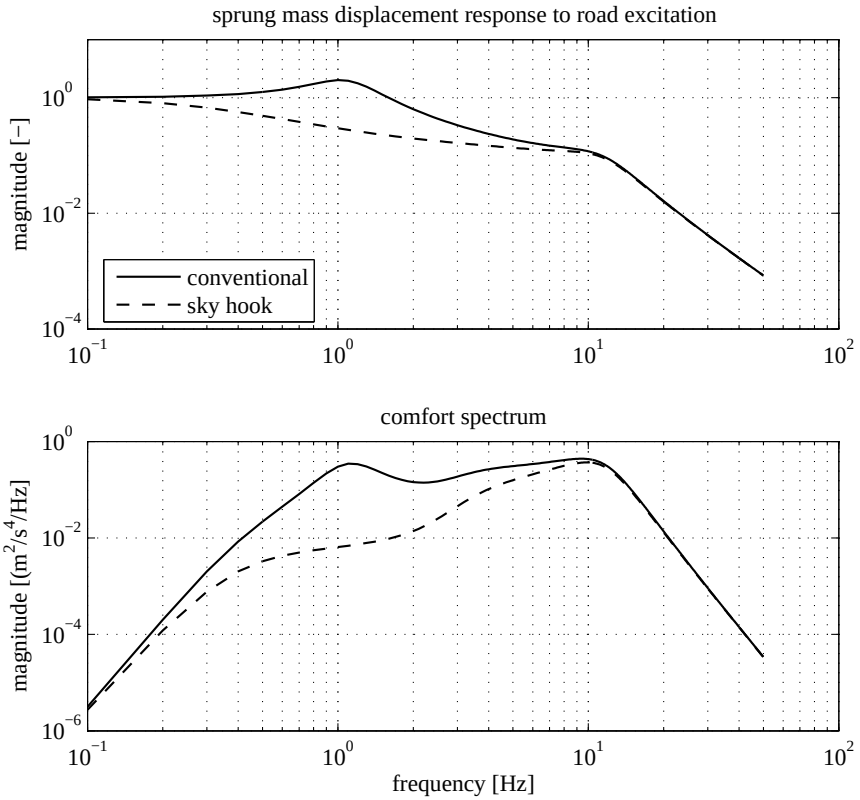

Figure 2.24: Sprung mass displacement responses to road excitations and comfort spectra of the original system and system equipped with a 'skyhook' damper

2.9 Skyhook damping: realization and control

In this section, it will be explained how a control law for an adjustable damper can be developed such that the working principle of a skyhook damper can be approximated. In figure 2.25, the damping forces acting on the sprung mass of the system with a skyhook

Table 2.9: Design parameters for the original and modified quarter car vehicle model showing the effect of having 'skyhook' damping

	original	modified ('skyhook')
ride comfort index	2.11 ms^{-2}	1.74 ms^{-2}
dynamic wheel load (RMS)	1512 N	1518 N
suspension travel (RMS)	21 mm	28 mm

damper are depicted. On the left, the force from the skyhook damper F_{sky} is shown; on the right, the force of the conventional damper F_d. The equations for the damping forces

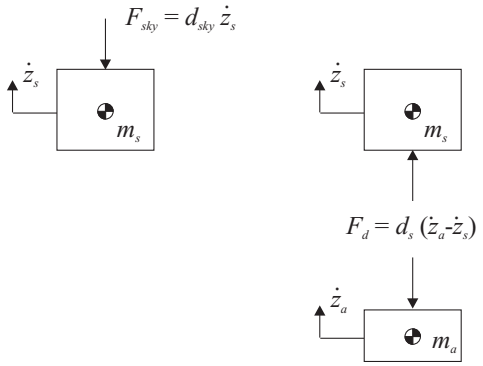

Figure 2.25: Damping forces acting on the sprung mass; left: (only) skyhook damper, right: conventional (adjustable) damper

read:

$$F_{sky} = d_{sky}\dot{z}_s \tag{2.57}$$

$$F_d = d_s(\dot{z}_a - \dot{z}_s) \tag{2.58}$$

We now assume that the damping constant d_s is adjustable ($0 < d_s < \infty$) and we want to generate the skyhook damper force using the adjustable damper:

$$F_d = d_s(\dot{z}_a - \dot{z}_s) = -d_{sky}\dot{z}_s \tag{2.59}$$

Note that (obviously) d_{sky} is positive. For positive values of the sprung mass velocity $\dot{z}_s$, we see that the adjustable damper force is compatible with the skyhook damper if $\dot{z}_s > \dot{z}_a$. For velocities $\dot{z}_a > \dot{z}_s$, the damper force is not compatible and we might switch of the damper ($d_s = 0$). On the other hand, if the sprung mass velocity $\dot{z}_s$ is negative, we find that the adjustable damper force is compatible with the skyhook damper if $\dot{z}_a > \dot{z}_s$. In that case, we may switch of the damper if $\dot{z}_s > \dot{z}_a$. With this in mind, the following control law is developed:

$$F_d = -d_{sky}\dot{z}_s \qquad \text{if} \qquad \dot{z}_s(\dot{z}_a - \dot{z}_s) < 0 \tag{2.60}$$

$$F_d = 0 \qquad \text{if} \qquad \dot{z}_s(\dot{z}_a - \dot{z}_s) > 0 \tag{2.61}$$

Notice that:

- The product $\dot{z}_s(\dot{z}_a - \dot{z}_s)$ also considers the sign of the sprung mass velocity!

- The velocity signals must be available...
- We have a nonlinear control law!

Simulink is used to build the quarter car vehicle model including the adjustable damper. Figure 2.26 depicts the model. The model details of the adjustable damper (skyhook

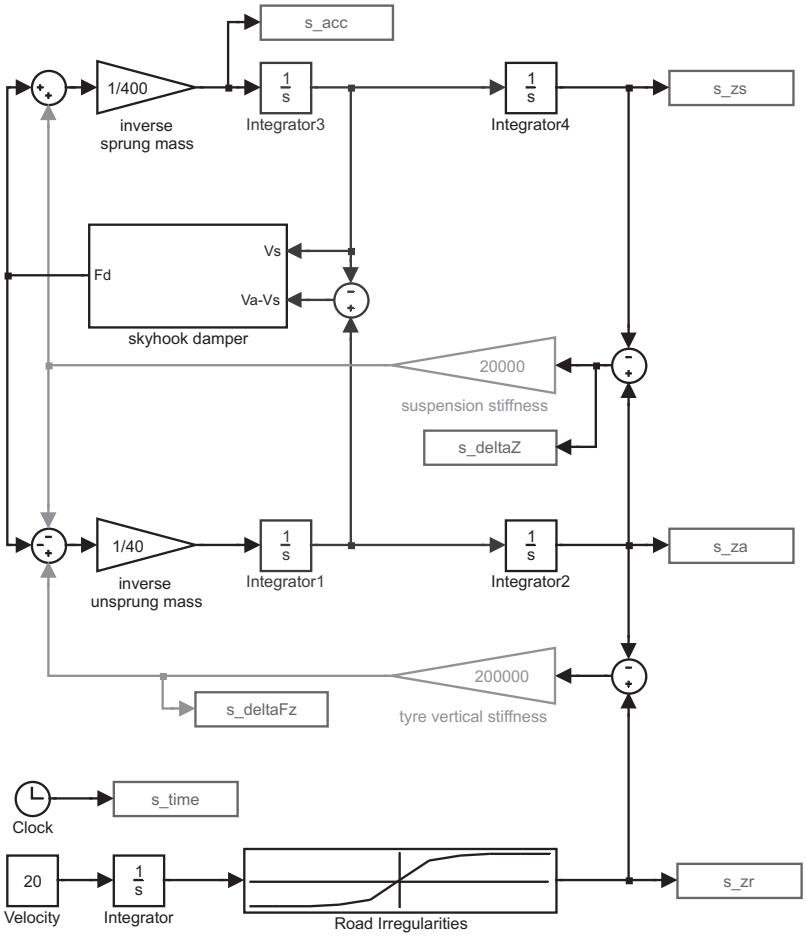

Figure 2.26: Matlab/Simulink model of the quarter car vehicle model including skyhook damper controller

damper block) are depicted in figure 2.27. Note that the switch block is used to account for the if-statement of equations (2.60) and (2.61). The simulation details are:

- Quarter car vehicle model parameters according to the model of section 2.2
- $d_{sky} = 5000$ Nsm^{-1}
- Measured road profile of figures 2.10 and 2.11 (right track)
- Forward velocity 20 ms^{-1} (72 kmh^{-1}), simulation time 60 s resulting in a traveled distance of 1200 m

Table 2.10 presents a comparison of the design parameters for the original system, the system with 'true' skyhook damper and the system with the adjustable/skyhook damper. As can be observed, the design parameters of the system with the skyhook damper are

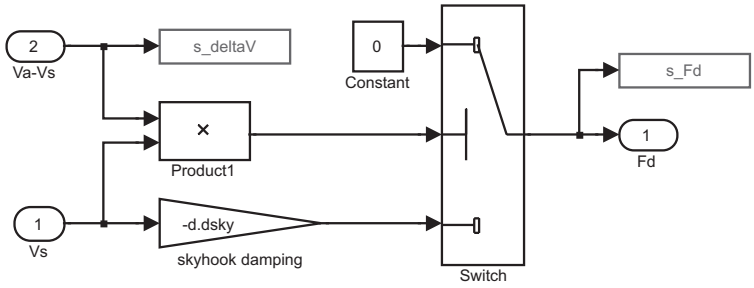

Figure 2.27: Detail of skyhook damper of the model of figure 2.26

rather close to those of the system with a 'true' skyhook damper, except the dynamic wheel loads. The RMS value of the dynamic wheel load of the system with skyhook damper is more than twice as big as that of the 'true' skyhook damper.

Table 2.10: Comparison of design parameters for the original system, the system with 'true' skyhook damper and the system with the adjustable/skyhook damper

	original	'true' skyhook	skyhook damper
acceleration (RMS) [ms^{-2}]	0.60	0.49	**0.37**
ride comfort index [ms^{-2}]	0.52	0.47	**0.29**
dynamic wheel load (RMS) [N]	**322**	**322**	727
suspension travel (RMS) [mm]	**5.5**	6.6	7.5

To illustrate the working of the skyhook damper, the accelerations of the system with the skyhook damper are compared with the accelerations of the original system in figures 2.28 and 2.29. Figure 2.28 presents the results in the time domain. Figure 2.29 shows

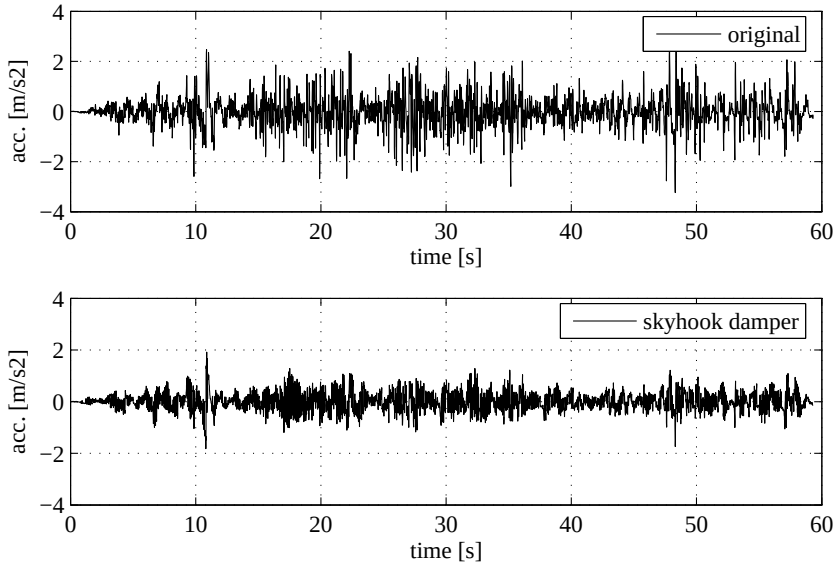

Figure 2.28: Comparison of acceleration signals of the original system and the system with skyhook damper

the probability density functions and the acceleration power spectral densities. From the figures, it is clear that the skyhook damper significantly reduces the acceleration amplitudes.

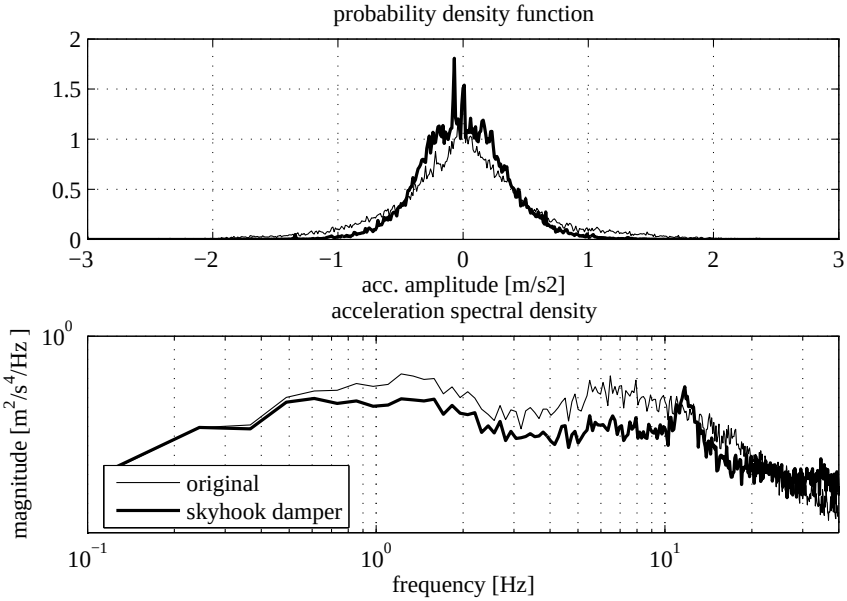

Figure 2.29: Probability density functions and power spectral densities of the accelerations of the sprung mass of the original system and the system with skyhook damper

Finally, the damper force is plotted versus the damper closing velocity in figure 2.30 for the conventional and the skyhook damper. Note that for the skyhook damper, the damper force equals zero in the upper left and lower right quadrant as result of the chosen control law.

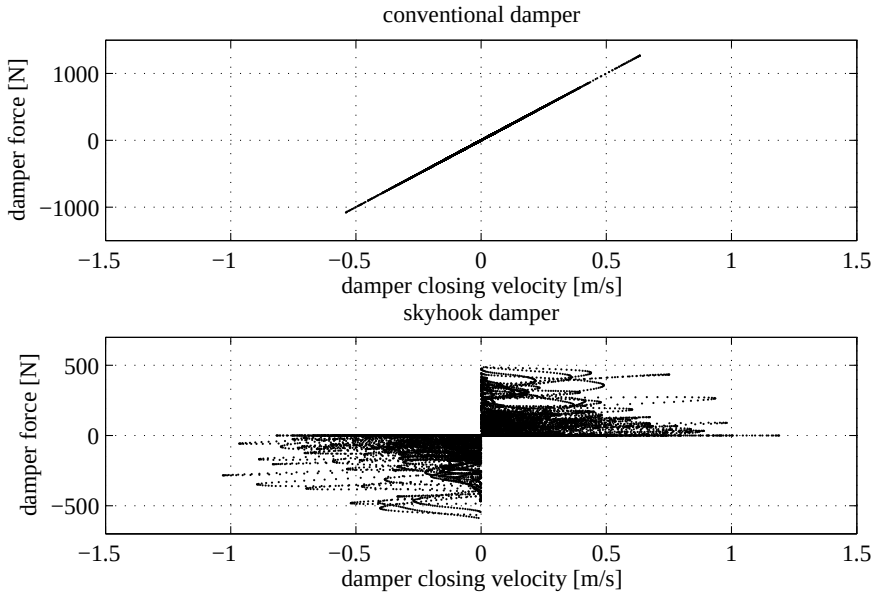

Figure 2.30: Damper force versus damper closing velocity for the system with a conventional damper and the system with a skyhook damper

Although the simulation results show that the accelerations of the sprung mass can be reduced considerably by using the skyhook damper, in practice there are two types of damper limitations that will deteriorate its performance. These two types of damper limitations are:

- The damping constant can only be adjusted within certain limits
- The damping constant cannot be adjusted infinitely fast

These two types of damper limitations will be discussed in detail hereafter.

Damping constant range limitations

The skyhook control law was developed under the assumption that the damping constant d_s is infinitely adjustable ($0 < d_s < \infty$). In real life however, the available range will be smaller:

$$d_{s,min} < d_s < d_{s,max} \tag{2.62}$$

Based on the damping force from the skyhook control law, we calculate the desired damping constant as follows:

$$d_{s,desired} = \frac{|F_{d,skyhook}|}{|\dot{z}_a - \dot{z}_s| + \epsilon} \qquad (\epsilon\text{: small number}) \tag{2.63}$$

Note that $F_{d,skyhook}$ is still obtained with equations (2.60) and (2.61). Next, we limit the desired damping constant to be within the available range:

$$d_{s,min} < d_{s,desired} < d_{s,max} \tag{2.64}$$

Finally, the damper force becomes:

$$F_d = d_{s,desired}(\dot{z}_s - \dot{z}_a) \tag{2.65}$$

This new skyhook damper is also implemented in the Simulink model. The skyhook damper model of figure 2.27 is replaced by the model of figure 2.31.

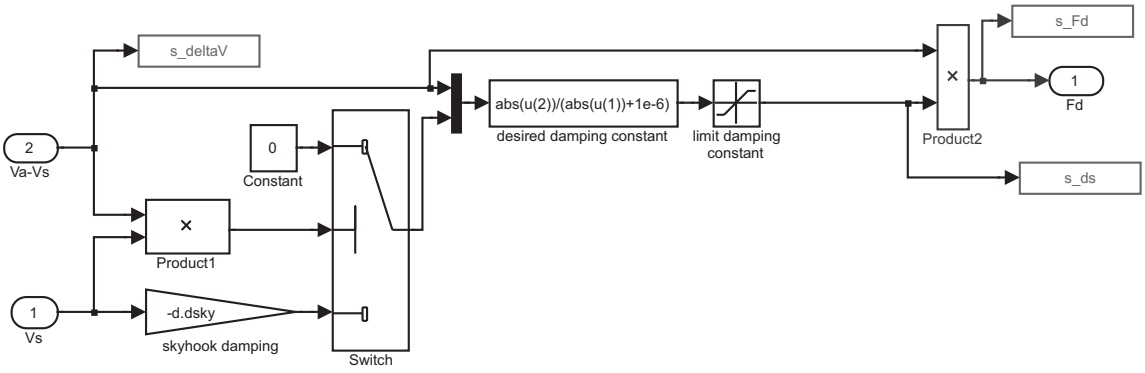

Figure 2.31: Detail of the skyhook damper model with damping constant range limitations

The following parameters are used:

- $d_{s,min} = 300$ Nsm^{-1}, $d_{s,max} = 3000$ Nsm^{-1}
- $\epsilon = 10^{-6}$

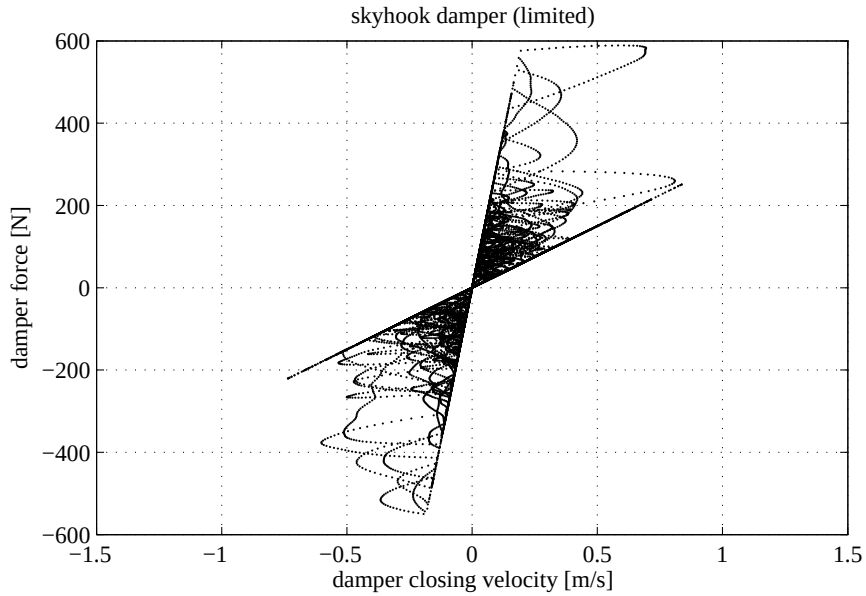

Figure 2.32: Damper force versus damper closing velocity for the system with skyhook damper with range limitations

Table 2.11: Comparison of design parameters for the original system, the system with 'true' skyhook damper, the system with skyhook damper and the system with skyhook damper with damping constant range limitations

	original	'true' skyhook	skyhook damper	skyhook damper (limited)
acceleration (RMS) [ms^{-2}]	0.60	0.49	**0.37**	0.38
ride comfort index [ms^{-2}]	0.52	0.47	**0.29**	0.30
dynamic wheel load (RMS) [N]	**322**	**322**	727	461
suspension travel (RMS) [mm]	**5.5**	6.6	7.5	6.4

The damper characteristics of the limited skyhook damper are shown in figure 2.32. Table 2.11 gives again a comparison of the design parameters. As can be observed in table 2.11, the skyhook damper still improves ride comfort significantly, whereas the dynamic tyre forces (ΔF_z) remain limited and have a reduction of required spring travel (Δz).

Response time limitations

As mentioned before, the damping constant cannot be adjusted infinitely fast. The reasons for the response time limitations are:

- Mechanical limitations, e.g. inertia
- Required bandwidth of the control system

To simulate a skyhook damper system with a limited response time, it is assumed that we can approximate the dynamics of switching the damping constant by means of a first-order

system with transfer function H:

$$H(s) = \frac{1}{\tau s + 1} \tag{2.66}$$

where τ is the time constant of the system. Figure 2.33 presents the result of a step response of a first-order system. Notice that now the system does not react infinitely fast anymore.

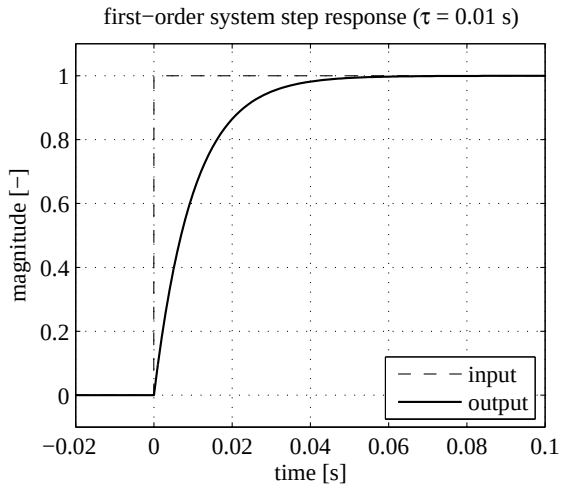

Figure 2.33: Step response of a first-order system

To include damper response time limitations in our Simulink model, the model of figure 2.31 is replaced by the model of figure 2.34.

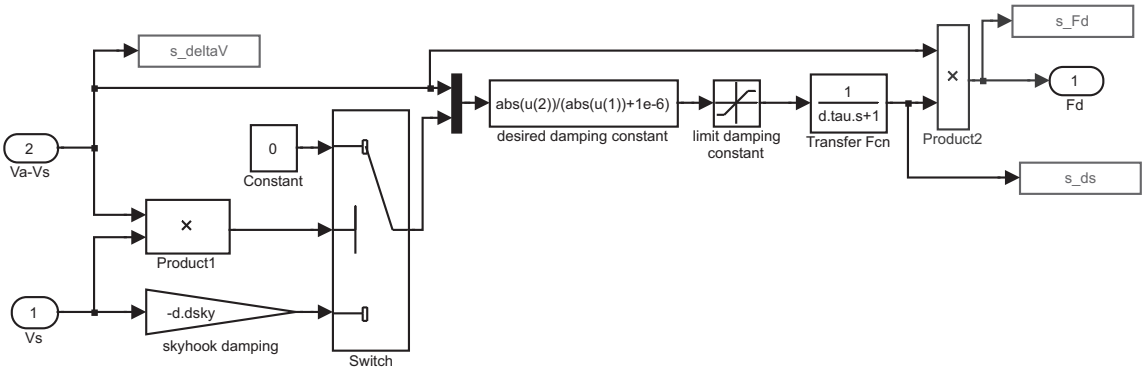

Figure 2.34: Detail of the skyhook damper model with damping constant range and response time limitations

In figure 2.35, the damping constant as function of time is plotted for the models including damping constant range and response time limitations. Table 2.12 presents the RMS values of the design parameters for different response times: 0, 5, 10 and 20 ms.
Some final notes:

- Due to limitations of the damper (damping constant range, response time), the performance gain in ride comfort is reduced with respect to the theoretical maximum

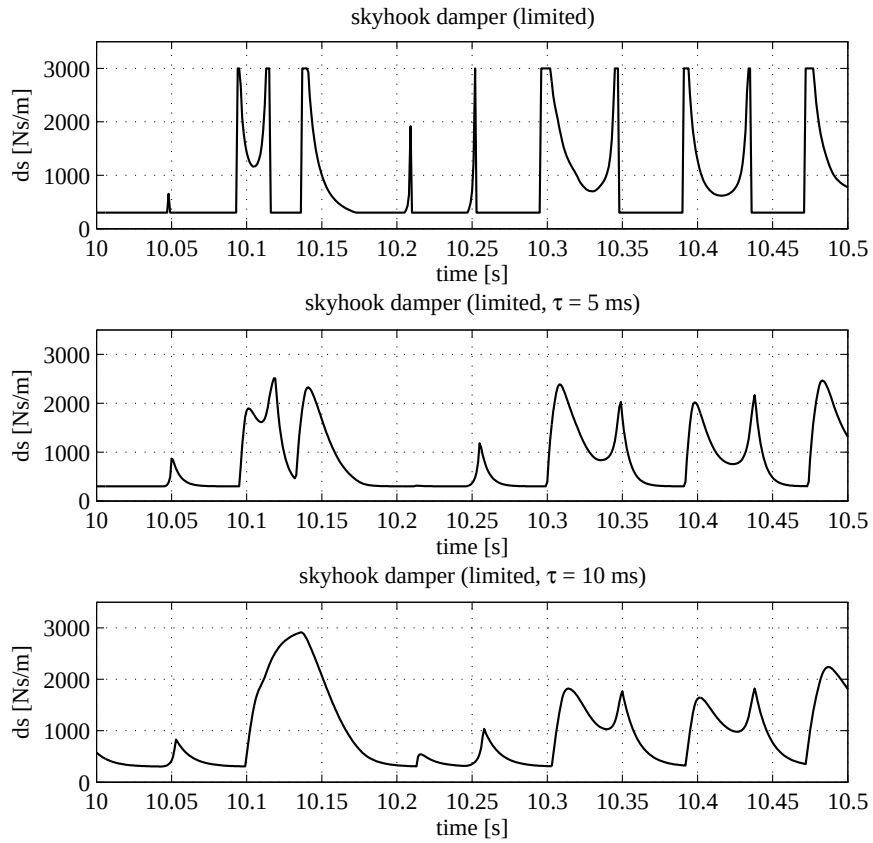

Figure 2.35: Damping constant d_s as function of time for the skyhook damper with damping constant limitations and three response times: 0, 5 and 10 ms

- Determination of the absolute velocity of the sprung mass ($\dot{z}_s$) accurately is also not trivial, since integrating signals from an accelerometer to obtain velocity often does not yield sufficiently accurate results, particularly at low frequencies

2.10 Active suspensions

In the examples of the previous section, a small amount of energy will be required for adjusting the damper constant and for the control system. The force acting on the sprung mass is generated using a passive element. Such a system is known as a ***semi-active suspension***. An alternative would be to apply the forces using an active element (e.g. a hydraulic actuator). In that case we would use all four quadrants of the force-relative velocity diagram (instead of two as in the semi-active case). Then we have an ***active suspension***, and it may require significant amounts of energy.

Active suspensions were 'hot' in the late 1980s and beginning of the 1990s, for example:

- Demonstrator cars developed by Lotus
- Used on F-1 racing cars (ride height control)
- Many (theoretical) papers

Table 2.12: Comparison of design parameters for the systems with damping constant range and response time limitations

	skyhook damper (limited)	skyhook damper (limited) $\tau = 5$ ms	skyhook damper (limited) $\tau = 10$ ms	skyhook damper (limited) $\tau = 20$ ms
acceleration (RMS) [ms^{-2}]	0.38	0.39	0.41	0.44
ride comfort index [ms^{-2}]	0.30	0.31	0.33	0.35
dynamic wheel load (RMS) [N]	461	445	421	396
suspension travel (RMS) [mm]	6.4	6.2	6.1	5.9

As already shown in the semi-active example, the control action due to delay in the response of the system may be too late and deteriorate the possible gains of the (semi-) active system. An idea to solve this problem is to use preview information: scan the road undulation ahead of the vehicle and take appropriate actions. See figure 2.36.

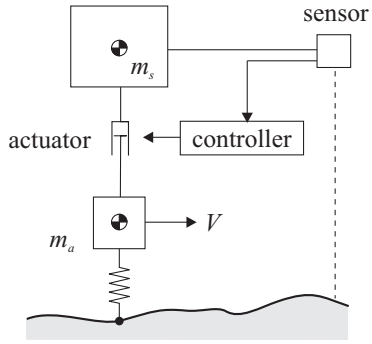

Figure 2.36: Active suspension system with preview

There is however one important problem: how to distinguish 'real' obstacles? It is easy to understand that problems will arise with the following obstacles: carton box, pothole filled with water, etc. A possible solution is to use the front axle as a sensor to detect the road undulations and use this preview information for the active control of the rear axle. For more details about this solution, it is referred to the PhD thesis of Huisman [4].
Examples of recent active suspension systems are:

- Mercedes ABC (Active Body Control)
  - series connection of hydraulic actuator and spring (avoid high frequency 'harshness')
  - controls vehicle body motions below 5 Hz
  - for higher frequency wheel vibrations, passive gas-pressure shock absorbers and coil springs are used, which can be tuned for high ride quality
- BMW Dynamic Drive
  - controls body roll
  - active anti-roll bars on the front and rear axles; active because rotating hydraulic actuators are integrated in the mechanical anti-roll bars
  - springs and dampers can be designed primarily for ride comfort

2.11 Half car model

Up to now, we only considered the quarter car vehicle model. This simple model does however not fully represent the rigid-body motions of a real car. Because of its wheelbase (i.e. the longitudinal distance between the axles), the real car is a multi-input system that responds with both bounce (vertical) and pitch (rotational) motions. Depending on the road profile and the forward velocity, either the bounce or pitch motion may be largely absent. To investigate this vehicle behavior we use the half vehicle model, which is shown in figure 2.37.

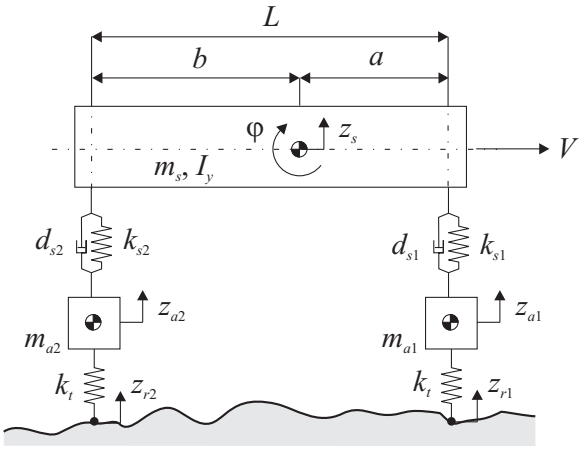

Figure 2.37: Half vehicle model

The equations of motion of this vehicle model read:

$$\mathbf{M\ddot{z} + D\dot{z} + Kz = Fu} \tag{2.67}$$

where:

$$\mathbf{z} = \begin{bmatrix} z_s & \varphi & z_{a1} & z_{a2} \end{bmatrix}^T \tag{2.68}$$

$$\mathbf{u} = \begin{bmatrix} z_{r1} & z_{r2} \end{bmatrix}^T \tag{2.69}$$

and ('*sym.*' denotes that the matrices are symmetric):

$$\mathbf{M} = \begin{bmatrix} m_s & 0 & 0 & 0 \\ 0 & I_y & 0 & 0 \\ 0 & 0 & m_{a1} & 0 \\ 0 & 0 & 0 & m_{a2} \end{bmatrix} \tag{2.70}$$

$$\mathbf{D} = \begin{bmatrix} d_{s1}+d_{s2} & -d_{s1}a+d_{s2}b & -d_{s1} & -d_{s2} \\ & d_{s1}a^2+d_{s2}b^2 & d_{s1}a & -d_{s2}b \\ & & d_{s1} & 0 \\ sym. & & & d_{s2} \end{bmatrix} \tag{2.71}$$

$$\mathbf{K} = \begin{bmatrix} k_{s1}+k_{s2} & -k_{s1}a+k_{s2}b & -k_{s1} & -k_{s2} \\ & k_{s1}a^2+k_{s2}b^2 & k_{s1}a & -k_{s2}b \\ & & k_{s1}+k_t & 0 \\ sym. & & & k_{s2}+k_t \end{bmatrix} \tag{2.72}$$

$$\mathbf{F} = \begin{bmatrix} 0 & 0 \\ 0 & 0 \\ k_t & 0 \\ 0 & k_t \end{bmatrix} \tag{2.73}$$

These equations can be translated easily into state-space form. As outputs we take the positions. The state-space equations read:

$$\mathbf{x} = \begin{bmatrix} \dot{\mathbf{z}} \\ \mathbf{z} \end{bmatrix} \tag{2.74}$$

$$\dot{\mathbf{x}} = \begin{bmatrix} -\mathbf{M^{-1}D} & -\mathbf{M^{-1}K} \\ \mathbf{I} & \mathbf{0} \end{bmatrix} \mathbf{x} + \begin{bmatrix} \mathbf{M^{-1}F} \\ \mathbf{0} \end{bmatrix} \mathbf{u} \tag{2.75}$$

$$\mathbf{y} = \begin{bmatrix} \mathbf{0} & \mathbf{I} \end{bmatrix} \mathbf{x} + \begin{bmatrix} \mathbf{0} \end{bmatrix} \mathbf{u} \tag{2.76}$$

Note that this system has 8 state variables, 2 inputs and 4 outputs. In order to analyse

Table 2.13: Half vehicle model parameters

Category	Parameters
Dimensions	$L = 2.7$ m; $a = 1.1$ m; $b = 1.6$ m
Masses and inertia	$m_s = 700$ kg; $I_y = 1000$ kgm^2; $m_{a1} = 45$ kg; $m_{a2} = 40$ kg
Suspension	$k_{s1} = 25000$ Nm^{-1}; $k_{s2} = 18000$ Nm^{-1}; $d_{s1} = 1800$ Nsm^{-1}; $d_{s2} = 1500$ Nsm^{-1}
Tyres	$k_t = 2e5$ Nm^{-1}

the model behavior, the set of parameters depicted in table 2.13 is used. The (damped) natural frequencies and damping ratios of the model equal:

- $f_d = 1.2$ Hz; $\zeta = 25\%$, bounce
- $f_d = 1.3$ Hz; $\zeta = 31\%$, pitch
- $f_d = 10.6$ Hz; $\zeta = 29\%$, front wheel hop
- $f_d = 11.1$ Hz; $\zeta = 26\%$, rear wheel hop

The mode shapes and natural frequencies of the system without damping are shown in figure 2.38. Notice that there is a small difference between the frequencies of the damped system and the system without damping. As can be observed in figure 2.38, there is a coupling of motions in the vertical and pitch directions, so that there are no 'pure' bounce and pitch modes. This is the case on most vehicles. Generally, we may denote the mode with predominantly vertical motions as bounce mode and the mode with predominantly angular motions as pitch mode. In figure 2.38 the bounce mode can be found at 1.2 Hz. In this case the center of rotation is outside the wheelbase. The pitch mode can be found at 1.3 Hz. Notice that for this mode the center of rotation is within the wheelbase.

We will now limit the discussion to the motions of the center of gravity as result of various combinations of road input:

- In phase vertical excitation:

$$z_{r1}(t) = z_{r2}(t) \tag{2.77}$$

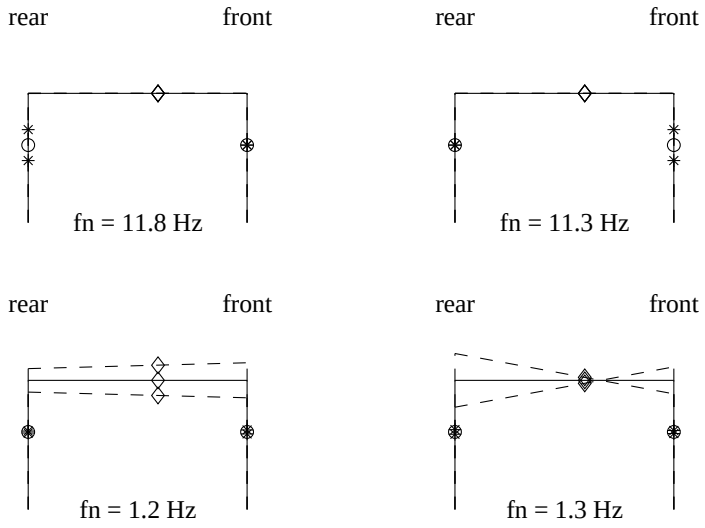

Figure 2.38: Mode shapes and natural frequencies of the half vehicle model without damping

- Out of phase vertical excitation:

$$z_{r1}(t) = -z_{r2}(t) \tag{2.78}$$

The transfer functions for the vertical displacement due to in phase and out of phase vertical excitation and the transfer functions for the pitch angle due to in phase and out of phase vertical excitation are shown in figure 2.39. Notice that in the plots for the vertical displacement to in phase excitation and the pitch angle to out of phase excitation, the magnitude of the transfer function for low frequencies is almost 1, whereas for the other two transfer functions the magnitude is considerably smaller than 1.

When driving over an uneven road, the rear wheels of the vehicle will encounter the same obstacles as the front wheels. This means that the road inputs for the front and rear axle are 100% correlated. Compared to the front wheel input, the input to the rear wheel experiences a time delay. This time delay τ is dependent on the forward velocity V and the wheelbase L:

$$\tau = \frac{L}{V} \tag{2.79}$$

Thus:

$$z_{r2}(t+\tau) = z_{r1}(t) \tag{2.80}$$

Making use of the Laplace transform properties for a pure time delay, the transfer function between the vertical road input and the various outputs equals:

$$H_{uy}(s) = H_{u1y}(s) + e^{-\tau s} H_{u2y}(s) \tag{2.81}$$

This relation is also shown in the block diagram of figure 2.40.
In figure 2.41, the magnitude of the transfer functions of the vertical displacement response of the center of gravity and the pitch angle response due to the vertical road displacement are plotted. In addition, the magnitudes of the transfer functions of the

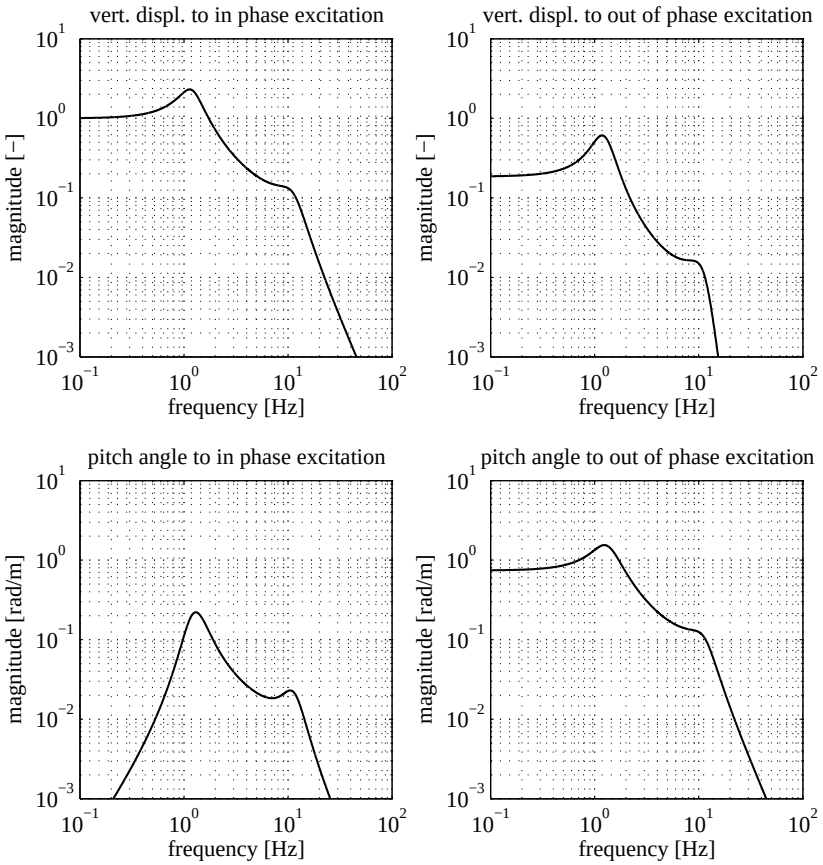

Figure 2.39: Transfer functions for the vertical displacement response and for the pitch angle response due to in phase and out of phase vertical excitations

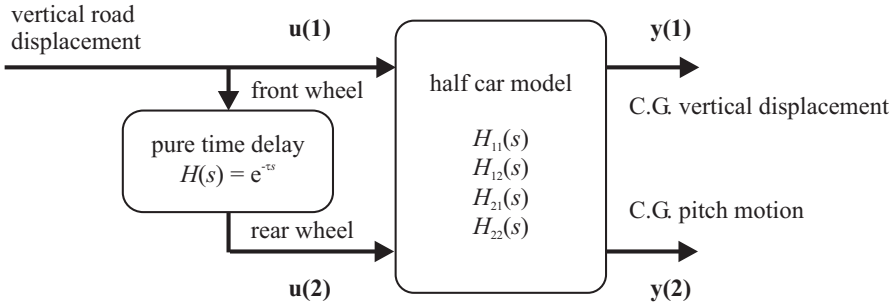

Figure 2.40: Input and output relations of the half vehicle model driving over an uneven road surface

vertical displacement response and the pitch angle response due to in phase and out of phase excitations, respectively, are plotted. The figure shows that for certain frequencies the magnitude of the transfer functions is almost zero. This effect is called ***wheelbase filtering***, because the location of the null points is related to the wheelbase of the vehicle. This will be explained below.
Consider a simple vehicle model consisting of a rod with end points (i.e. wheels) that

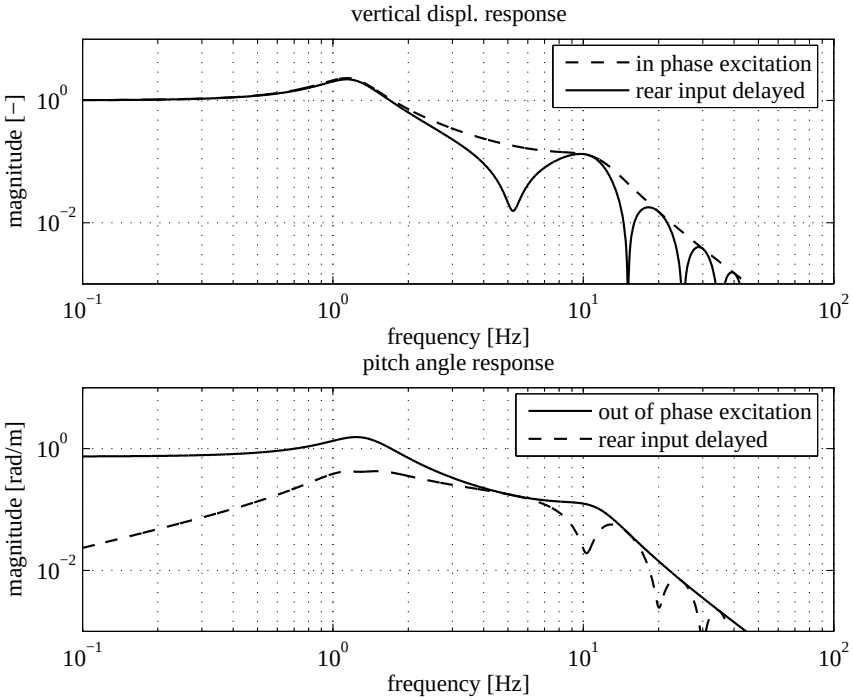

Figure 2.41: Transfer functions for the vertical displacement response and for the pitch angle response due to vertical excitation

move over a road profile. Imagine that the vehicle (i.e. rod) moves over a road profile, which contains all wavelengths. In this case, we can examine the response of the vehicle to individual wavelengths. It appears that no vertical or pitch motion exists for certain ratios of wheelbase and road surface wavelength. These cases are depicted in figure 2.42. The figure indicates that the vertical displacement of the center of our simple vehicle

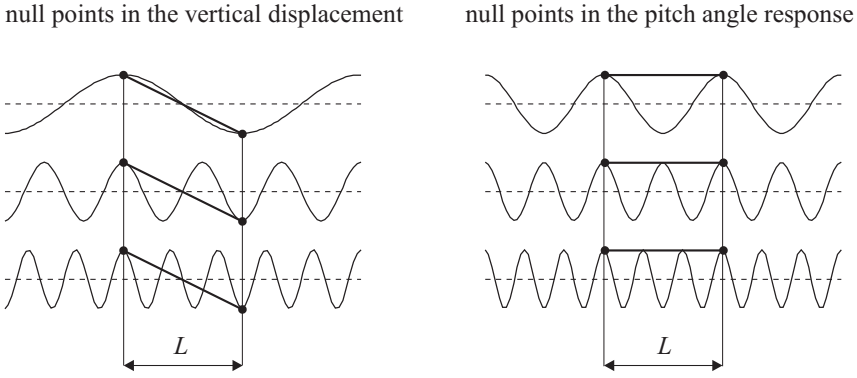

Figure 2.42: Explanation of the origin of null points in the vertical displacement and pitch angle response

model is unresponsive, i.e. equals zero, if the wheelbase equals half the wavelength of the road profile or any odd multiple times half the wavelength of the road profile. The pitch angle is unresponsive if the wheelbase equals the wavelength of the road profile or any integer multiple times the wavelength of the road profile. The fact that the vehicle

is unresponsive for certain wavelengths leads to null points in the transfer functions of the vertical displacement and pitch angle. The frequencies f_{null} of the null points in the transfer functions can be calculated with the following equations:

$$f_{null,vertical} = \frac{V}{\lambda_{null,vertical}} = \frac{(2n-1)V}{2L} \qquad \text{with:} \quad n = 1, 2, 3, ... \tag{2.82}$$

$$f_{null,pitch} = \frac{V}{\lambda_{null,pitch}} = \frac{nV}{L} \qquad \text{with:} \quad n = 0, 1, 2, 3, ... \tag{2.83}$$

In our example, the forward velocity of the vehicle is chosen to be 27 ms^{-1}. The wheelbase of our vehicle is 2.7 m. Consequently, we find null points at 5, 15, 25,... Hz in the transfer function of the vertical displacement and null points at 0, 10, 20, 30,... Hz in the transfer function of the pitch angle. Finally, notice that as a result of wheelbase filtering the ride comfort index may not always increase with forward velocity!!

2.12 Nonlinear behavior

So far only linear behavior was considered. In reality, most vehicle components exhibit a nonlinear behavior. Therefore, the major nonlinearities of the vehicle suspension system are discussed briefly in this section.

Suspension stiffness

When considering the vertical stiffness characteristic of a suspension (see figure 2.43) a number of nonlinearities can be observed:

- Bump and rebound stops: elastic members that increase the wheel rate toward the end of the suspension travel; much stiffer than the main spring
- Stiffness of the main spring may be progressive with deflection
- Main spring may be mounted under preload

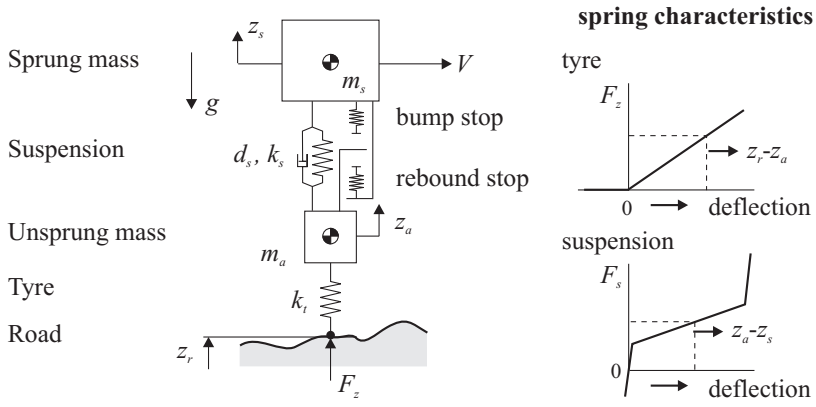

Figure 2.43: Major suspension nonlinearities

Shock absorber

In practice, the shock absorber has a highly nonlinear, asymmetric characteristic (even for small amplitudes):

- low damping coefficient on compression (jounce)
- high damping coefficient on extension (rebound)

See for example figure 2.44. In practice, damper fine-tuning is generally done on prototype vehicles by experienced test drivers.

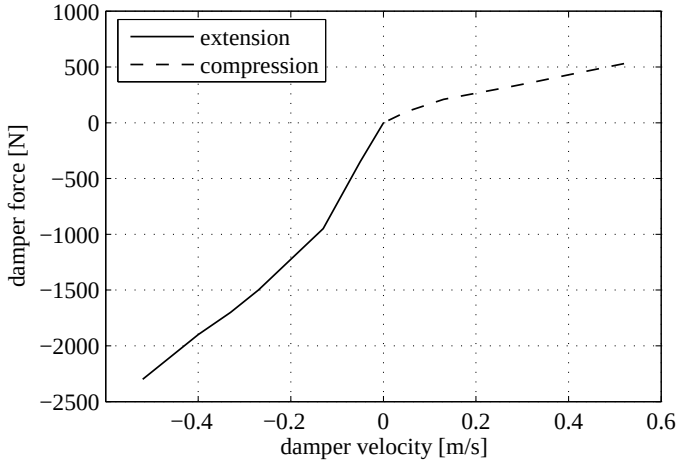

Figure 2.44: Nonlinear shock absorber characteristic

Friction

Depending on the suspension design, the vertical motion of the wheel will experience a significant amount of dry friction. For example, in a McPherson strut the normal forces on the bearings can result in significant friction forces opposing the compression/extension of the strut. This is illustrated in figure 2.45. Possible solutions to minimize the influence

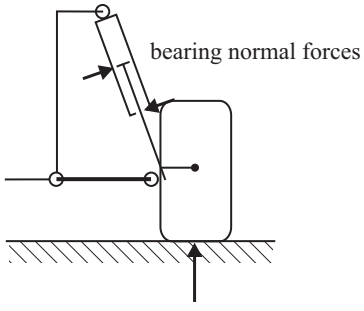

Figure 2.45: In a McPherson strut, the normal forces on the bearings can result in significant friction forces opposing the compression/extension of the strut

of these friction forces are:

- optimize the geometry, i.e. minimize the normal forces on the bearings
- use a bearing material with a low friction coefficient

Tyre vertical behavior

The tyre vertical behavior is nonlinear in the following ways:

- A tyre is almost a linear spring; the vertical stiffness increases slightly with deflection
- Vertical tyre force F_z cannot become negative, because the tyre loses contact with the road
- For a rolling tyre, the amount of damping is rather small (and may be neglected)
- A non-rolling tyre has a fair amount of hysteresis (figure 2.46)
- Tyre vertical stiffness increases with rotational velocity

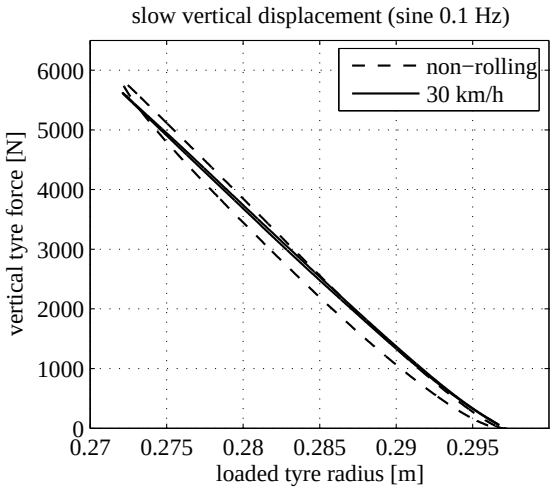

Figure 2.46: Vertical stiffness characteristic for a rolling and a non-rolling tyre, showing the difference in hysteresis

The order of magnitude of the vertical stiffness and damping for a passenger car tyre are:

- spring stiffness: 200000 Nm^{-1} (200 Nmm^{-1})
- damping: 50 Nsm^{-1} (rolling tyre)

Tyre enveloping behavior

For long wavelength obstacles (much longer than the tyre contact length), a single point contact model (single vertical spring for the tyre) may be sufficient. For short wavelength obstacles, the 'enveloping' behavior of the tyre has to be taken into account. What is meant with enveloping behavior can be explained best on the basis of an example. In figure 2.47, the responses of a tyre are shown when the tyre is rolled quasi-statically over an obstacle with length much smaller than the tyre contact length at constant velocity and axle height. Three distinct responses can be observed:

- variations in the vertical force
- variations in the longitudinal force
- variations in the spin velocity of the wheel

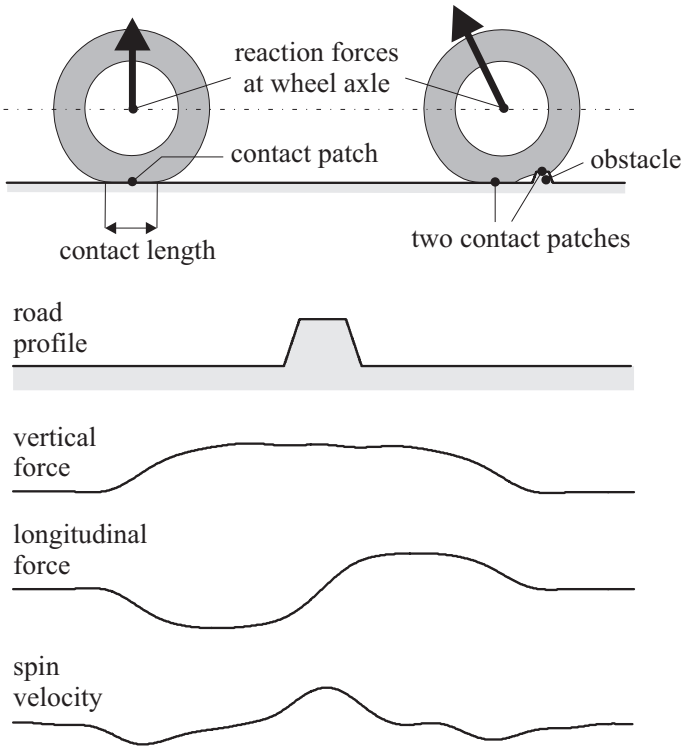

Figure 2.47: Example of tyre enveloping behavior [7]

The figure shows that these three responses are much longer than the length of the obstacle. This is caused by the elastic properties and geometry of the tyre. Due to its contact length and curvature in the contact zone, the tyre touches the obstacle before the wheel center will pass it. Visa versa, the tyre still touches the obstacle after that the wheel center has passed it. In the figure, it is also illustrated that the tyre deforms around the obstacle due to its elastic properties. In the sketched situation for example, two contact patches exist. These phenomena result in a response of the tyre that is much smoother than the obstacle shape. One often says that the tyre filters the obstacle.

A feasible procedure to handle these short wavelength obstacles is to translate the geometrical road profile into an ***'effective road profile'***. A single point contact model can then be used in combination with the effective road profile to calculate the vehicle response. An example of the effective road surface for a step is shown in figure 2.48. For more details about the effective road surface and suitable enveloping models, which can be used to obtain the effective road surface, it is referred to the PhD theses of Schmeitz [7] and Zegelaar [8]. When comparing the effective with the actual road profile, it is clear that the quarter car step response as e.g. presented in figures 2.6 and 2.7 may actually be different. In figure 2.49, the step responses of the quarter car vehicle model moving over the pure step and the effective road profile (for this step) are compared. As can be observed, the response amplitudes for the model with the pure step directly as input of the model are too large.
Some notes:

- At higher forward velocities the differences become smaller again, but for higher obstacles the differences will increase
- Dynamics (vibrations) of the tyre belt are ignored in this simplified example; a detailed discussion is outside the scope of this lecture

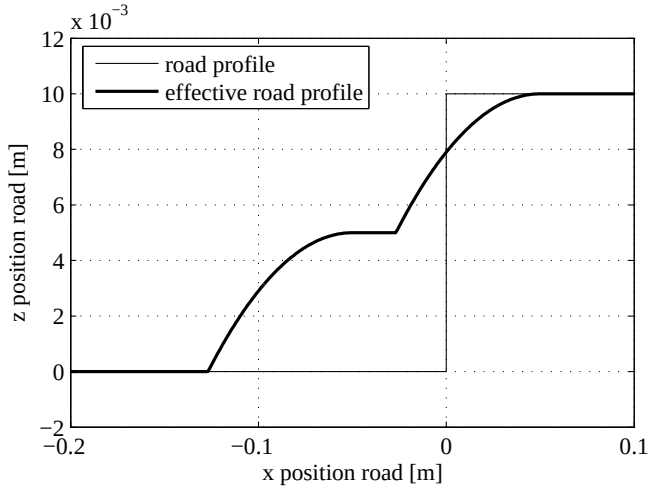

Figure 2.48: Effective road profile for a step obstacle

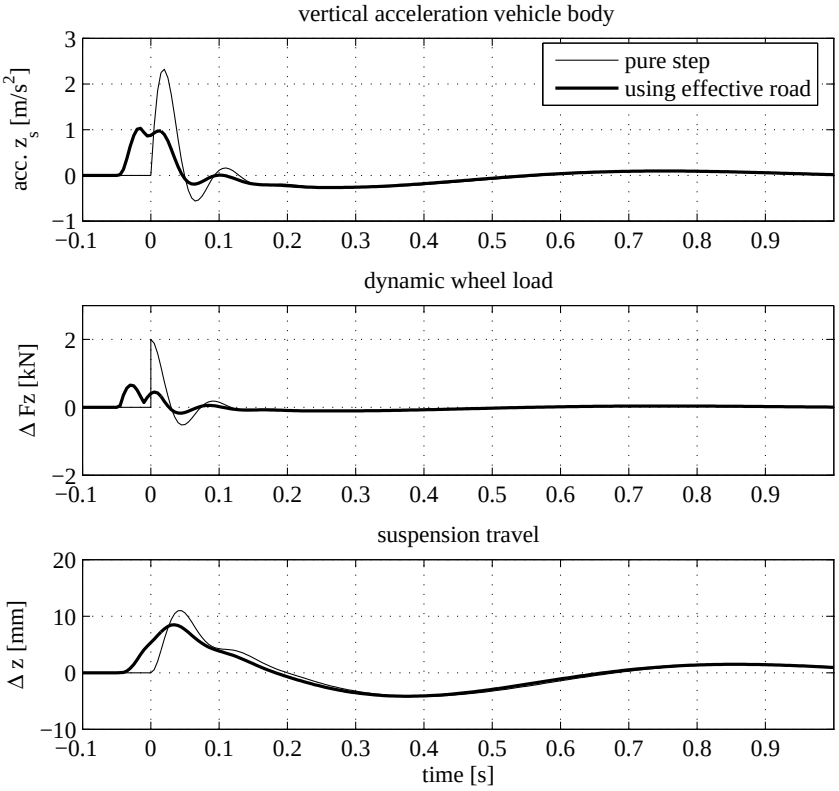

Figure 2.49: Comparison of quarter car vehicle model responses to a step in road profile using the effective road profile or the actual road profile as input (velocity 10 ms^{-1}, step height 10 mm)

Finally, the main consequence of tyre enveloping behavior is that the amplitudes of short wavelength obstacles (so the road input at high excitation frequencies) are reduced. In figure 2.50 for example, the power spectral densities of a quarter car vehicle model (including a rigid ring dynamic tyre model) with and without enveloping model are

compared with the PSD of measurements when driving with 72 kmh^{-1} over a rough road profile. The figure clearly shows that including tyre enveloping behavior in the model significantly improves the results. It is also shown that in the frequency domain the tyre acts like a lowpass filter.

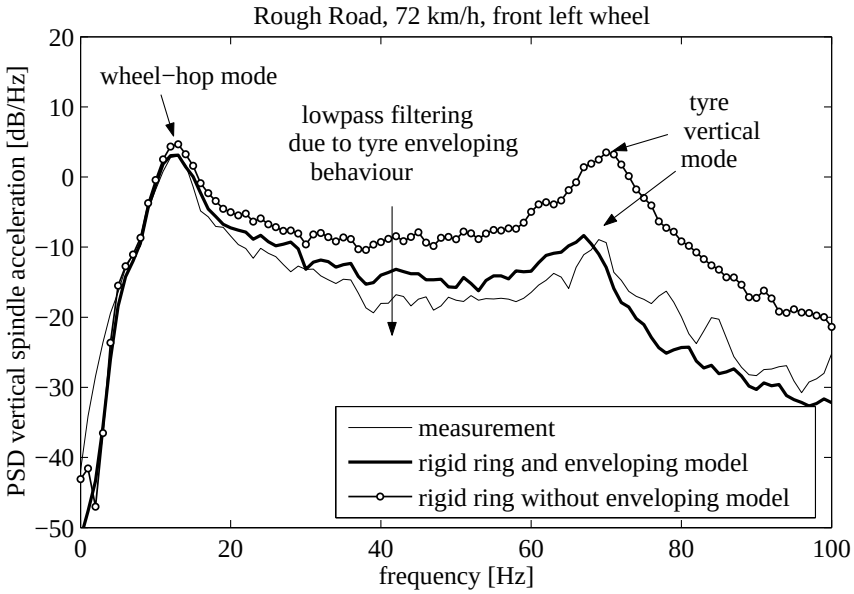

Figure 2.50: Comparison of power spectral densities of the vertical axle acceleration, showing that including tyre enveloping behavior significantly improves simulation results [7]

References

[1] ISO 8608 (1995). Mechanical vibration - road surface profiles - reporting of measured data. *International Standard*, 1995.

[2] ISO 2631-1 (1997). Mechanical vibration and shock - evaluation of human exposure to whole-body vibration, part 1, general requirements. *International Standard*, 1997.

[3] T.D. Gillespie. *Fundamentals of Vehicle Dynamics*. Society of Automotive Engineers, 1992.

[4] R.G.M. Huisman. *A Controller and Observer for Active Suspensions with Preview*. PhD thesis, Eindhoven University of Technology, Eindhoven, The Netherlands, 1994.

[5] A. de Kraker. *A Numerical-Experimental Approach in Structural Dynamics, lecture notes*. Eindhoven University of Technology, Eindhoven, The Netherlands, 2000.

[6] I. Rericha. Methoden zur objektiven bewertung des fahrkomforts. *Automobil-Industrie*, 2/86:175–182, 1986.

[7] A.J.C. Schmeitz. *A Semi-Empirical Three-Dimensional Model of the Pneumatic Tyre Rolling over Arbitrary Uneven Road Surfaces*. PhD thesis, Delft University of Technology, Delft, The Netherlands, 2004.

[8] P.W.A. Zegelaar. *The Dynamic Response of Tyres to Brake Torque Variations and Road Unevennesses*. PhD thesis, Delft University of Technology, Delft, The Netherlands, 1998.